

Biogeochemistry and Community Composition of Iron- and Sulfur-Precipitating Microbial Mats at the Chefren Mud Volcano (Nile Deep Sea Fan, Eastern Mediterranean)[∇]

Enoma O. Omoregie,^{1,2,*} Vincent Mastalerz,³ Gert de Lange,³ Kristina L. Straub,^{4,†} Andreas Kappler,⁴ Hans Røy,¹ Alina Stadnitskaia,⁵ Jean-Paul Foucher,⁶ and Antje Boetius^{1,2,7*}

Max Planck Institute for Marine Microbiology, Bremen, Germany¹; Jacobs University, Bremen, Germany²; Department of Earth Sciences, Utrecht University, Utrecht, The Netherlands³; Center for Applied Geosciences, Eberhard Karls University, Tübingen, Germany⁴; Royal Netherlands Institute for Sea Research (NIOZ), Texel, The Netherlands⁵; Department of Marine Geosciences, IFREMER Centre de Brest, Plouzane Cedex, France⁶; and Alfred Wegener Institute for Polar and Marine Research, Bremerhaven, Germany⁷

Received 27 July 2007/Accepted 29 February 2008

In this study we determined the composition and biogeochemistry of novel, brightly colored, white and orange microbial mats at the surface of a brine seep at the outer rim of the Chefren mud volcano. These mats were interspersed with one another, but their underlying sediment biogeochemistries differed considerably. Microscopy revealed that the white mats were granules composed of elemental S filaments, similar to those produced by the sulfide-oxidizing epsilonproteobacterium “*Candidatus Arcobacter sulfidicus*.” Fluorescence in situ hybridization indicated that microorganisms targeted by a “*Ca. Arcobacter sulfidicus*”-specific oligonucleotide probe constituted up to 24% of the total the cells within these mats. Several 16S rRNA gene sequences from organisms closely related to “*Ca. Arcobacter sulfidicus*” were identified. In contrast, the orange mat consisted mostly of bright orange flakes composed of empty Fe(III) (hydr)oxide-coated microbial sheaths, similar to those produced by the neutrophilic Fe(II)-oxidizing betaproteobacterium *Leptothrix ochracea*. None of the 16S rRNA gene sequences obtained from these samples were closely related to sequences of known neutrophilic aerobic Fe(II)-oxidizing bacteria. The sediments below both types of mats showed relatively high sulfate reduction rates ($300 \text{ nmol} \cdot \text{cm}^{-3} \cdot \text{day}^{-1}$) partially fueled by the anaerobic oxidation of methane (10 to $20 \text{ nmol} \cdot \text{cm}^{-3} \cdot \text{day}^{-1}$). Free sulfide produced below the white mat was depleted by sulfide oxidation within the mat itself. Below the orange mat free Fe(II) reached the surface layer and was depleted in part by microbial Fe(II) oxidation. Both mats and the sediments underneath them hosted very diverse microbial communities and contained mineral precipitates, most likely due to differences in fluid flow patterns.

Submarine mud volcanoes are geological structures formed by episodic eruption of gases and muds from deep subsurface reservoirs. Some mud volcanoes continuously expel reduced muds, fluids, and gases into the ocean, supplying chemical energy to cold seep organisms, such as dense mats of giant sulfur-oxidizing bacteria, siboglinid tubeworms, and a variety of bivalves (71). Active mud volcanoes with such cold seep ecosystems are known from the Central Mediterranean Ridge (14, 62, 92), the Central American continental margin (50), the Gulf of Cadiz (58), and the Barents Sea (59). In the Eastern Mediterranean, active mud volcanism associated with diverse ecosystems has recently been detected on the Nile Deep Sea Fan (14, 40, 47; E. O. Omoregie, H. Niemann, V. Mastalerz, G. de Lange, A. Stadnitskaia, J. Mascle, J.-P. Foucher, and A. Boetius, submitted for publication).

At mud volcanoes, as well as at many other cold seeps, methane and sometimes higher hydrocarbons are transported upward with rising fluids and muds and can escape into the hydrosphere in the form of gas or oil bubbles (51, 59, 68). Anaerobic hydrocarbon degradation forms the basis of a steep sequence of biogeochemical processes connecting the carbon and sulfur cycles at these sites (1, 69). When hydrocarbons reach the sulfate-penetrated sediment zones, they are utilized by sulfate-reducing bacteria (SRB) as energy and carbon sources. The products of sulfate respiration with methane and higher hydrocarbons are sulfide and bicarbonate (1, 7, 28). Hence, hydrocarbon seepage is generally associated with high sulfide fluxes (59, 81). At methane seeps, most of the sulfide is produced via the anaerobic oxidation of methane (AOM) mediated by anaerobic methanotrophic archaea (ANME) (reference 21 and references therein). However, several oily cold seep systems have been discovered (28, 58), including some in the Eastern Mediterranean (Omoregie et al., submitted), where anaerobic oxidation of higher hydrocarbons coupled to sulfate reduction is the dominant sulfide source.

Sulfide is central to biogeochemical cycling in marine sediments as an energy-rich microbial substrate and the principal product of one of the most quantitatively important respiratory processes in ocean sediments, namely, sulfate reduction (32). Sulfide reacts spontaneously with Fe(III) and Fe(II) (80) and

* Corresponding author. Present address for Enoma O. Omoregie: School of Earth, Atmospheric and Environmental Sciences, The University of Manchester, Manchester, United Kingdom. Phone: (44) 161-275-5668. Fax: (44) 0161-306-9361. E-mail: enoma.omoregie@manchester.ac.uk. Mailing address for Antje Boetius: Max Planck Institute for Marine Microbiology, Bremen, Germany. Phone: (49) 421 2028 860. Fax: (49) 421 2028 690. E-mail: aboetius@mpi-bremen.de.

† Present address: Department of Biogeochemistry, Vienna University, Vienna, Austria.

[∇] Published ahead of print on 31 March 2008.

with Mn(II) and Mn(IV) (9) and is used as an electron donor in a variety of aerobic and anaerobic sulfide-oxidizing microorganisms. Well-known marine sulfide-oxidizing organisms include the giant vacuolated *Gammaproteobacteria*, such as *Beggiatoa* and *Thiomargarita* spp., which use oxygen or nitrate for respiration and often form dense mats above hydrocarbon seeps (7, 29, 59, 61). Other types of sulfide-oxidizing bacteria that are mostly known from hydrothermal vent systems but are also found sporadically in cold seep systems belong to the *Epsilonproteobacteria* (10). Little is known about the nature and functioning of other types of bacteria and archaea which appear to be commonly associated with cold seep ecosystems, such as the crenarchaeotal groups marine benthic group B (MBGB) and MBG1 (35, 36, 52).

Here we report on our investigation of the biogeochemistry and microbial community structure of two types of closely associated bacterial mats. These mats were discovered during a dive with the submersible *Nautille* (IFREMER) to a brine-impacted cold seep at the bottom of the Chefren mud volcano located in a large caldera of the western Nile Deep Sea Fan (Menes Caldera). Similar types of mats have been seen at hydrothermal vents (16, 74, 77) but to date have not been described in association with cold seeps. In this study we combined microscopic, biogeochemical, and molecular analyses to identify the underlying factors that cause the formation of these two distinct mat systems. This work was part of the ESF EUROCORES EUROMARGIN project MEDIFLUX, which is an integrated study of fluid and gas seepage through the seabed of the Nile Deep Sea Fan.

MATERIALS AND METHODS

Sampling location. The Chefren mud volcano of the MENES Caldera was discovered by bathymetry surveys of the western Nile Deep Sea Fan during the "FANIL" expedition in 2000 (48). Its sediments were sampled for the first time during the "NAUTINIL" expedition (this study) with the RV *L'Atalante* and submersible *Nautille* (IFREMER) in September 2003. The Menes Caldera (Fig. 1A) is an 8-km-diameter circular depression that is approximately 50 to 100 m deep and is located at a water depth of about 3,000 m in the western province of the Nile Deep Sea Fan. This caldera contains three mud volcanoes, Chefren, Cheops, and Mykerinos (Fig. 1B). Chefren is about 500 m in diameter and rises to about 60 m above the bottom of the caldera (3,020 m) (Fig. 1C). At the time of sampling the center of this mud volcano was filled by a large and deep brine and mud lake. A more detailed description of the Menes Caldera and associated structures will be given elsewhere (C. Huguen, J. P. Foucher, J. Mascle, H. Ondreas, M. Thouement, S. Gonthat, A. Stadnitskaia, C. Pierre, G. Bayon, L. Loncke, A. Boetius, I. Bouloubassi, G. de Lange, Y. Fouquet, J. Woodside, and N. S. Party, submitted for publication).

Sampling. Sediment samples were recovered from orange and white mats by the submersible *Nautille* (32°06.74'N, 028°10.35'E; water depth, 3,024 m) (Fig. 2A and B). The samples were collected using 6-cm-diameter push cores. Two push cores were taken from the orange mat [cores NL18PC1(8) and NL18PC2(7)] (Fig. 2E), and two push cores were taken from the white mat above black sediments [cores NL18PC3(5) and NL18PC4(6)] (Fig. 2D); in addition, two blade cores [NL18BC1(L3) and NLBC2(L7)] were taken from the nearby sediments. When cores were returned to the RV *L'Atalante*, they were immediately taken to the cold room, and 1-cm-diameter subcores were taken and used for further analyses as described below. Cores NL18PC3(5) and NL18PC1(8) were used for microbiological analyses, as well as rate measurements, whereas cores NL18PC4(6) and NL18PC2(7) were used for geochemical analyses. Due to the exploratory nature of the expedition, samples were limited to material obtained during one dive.

Methane concentration. Subcores were sectioned and preserved with 2.5% NaOH in rubber-sealed glass vials. Methane concentrations were measured by injecting 100 μ l of the headspace gas into a Hewlett Packard 5890A gas chromatograph.

Methane oxidation rate determination. Methane oxidation rates were measured using ^{14}C CH₄ gas, based on previously described methods (24, 81). Subcores were injected with 10 μ l of ^{14}C CH₄ (2.5 kBq [total radioactivity] dissolved in double-distilled H₂O) and incubated for 24 h in the dark at the in situ temperature, 14°C. Following incubation the cores were sectioned and fixed with 2.5% NaOH. Further processing was done as described by Treude et al. (81). AOM rates were determined using the following equation: AOM rate = $[\text{TR}^{14}\text{CO}_2/(\text{TR}^{14}\text{CO}_2 + \text{TR}^{14}\text{CH}_4)] \cdot [\text{CH}_4]/V/t$, where ^{14}C CO₂ is the activity of CO₂ produced, ^{14}C CH₄ is the activity of the residual injected ^{14}C CH₄, [CH₄] is the CH₄ concentration, V is the sediment volume, and t is time.

SR rate determination. Sulfate reduction (SR) rates were obtained using ^{35}S SO₄²⁻ and previously described methods (27). Subcores were injected with 5 μ l ^{35}S SO₄²⁻ (100 kBq [total radioactivity] dissolved in double-distilled H₂O) and incubated for 24 h at the in situ temperature in the dark. Following incubation, the sediment was sectioned and placed in a polypropylene tube containing 20% zinc acetate. Further processing was done as described by Kallmeyer et al. (30). SR rates were calculated using the following equation: SR rate = $[\text{TR}^{35}\text{S}/(\text{TR}^{35}\text{S} + \text{TR}^{35}\text{SO}_4^{2-})] \times [\text{SO}_4^{2-}]/V/t$, where TR³⁵S is the activity of total reduced inorganic sulfur, ^{35}S SO₄²⁻ is the activity of the residual ^{35}S SO₄²⁻ tracer, [SO₄²⁻] is the SO₄²⁻ concentration in the sample, V is the sediment volume, and t is time.

Geochemical measurements. For sulfide analysis, 10 μ l of 0.1 N NaOH was added to 2-ml pore water subsamples. Subsamples were analyzed on board using a TRAACS800 continuous-flow analyzer and colorimetric methods described by Grasshoff et al. (20). Pore water major element analyses were conducted using inductively coupled plasma atomic emission spectroscopy; 2-ml subsamples were acidified by adding 100 μ l of suprapur HNO₃ (1 M), bubbled to remove sulfide, and stored in the dark at 4°C. Sulfate concentrations were measured by analyzing S. The standard deviation for all measurements was <3%. The geochemical composition of the solid phase was also determined by inductively coupled plasma atomic emission spectroscopy after total dissolution of sediments in an acid mixture containing HClO₄, HNO₃, and HF (64). The organic carbon content was determined using the method described by van Santvoort et al. (85). International and in-house standards and duplicates were processed to monitor precision and accuracy. Note that very little pore water was recovered from the 7- to 9-cm sample from the orange mat; therefore, a high error is likely associated with values for this sample.

Light and epifluorescence microscopy. Sediment sections were preserved in 2% formalin and artificial seawater for acridine orange (AO) staining, as well as for light microscopy. Samples for fluorescence in situ hybridization (FISH) were initially fixed in a 2% formalin-seawater solution, washed several times with phosphate-buffered saline, and finally stored in a phosphate-buffered saline-ethanol solution (1:1). Specific groups of *Bacteria* and *Archaea* were quantified using catalyzed reporter deposition FISH (CARD-FISH); the exceptions were ANME-2 and aerobic methanotrophic bacteria (M γ 705 probe) (15), for which monolabeled FISH probes were used because no results were obtained with CARD-FISH probes. AO staining (6), FISH (73), and CARD-FISH (23) were all performed using previously described methods. All FISH and CARD-FISH slides were counterstained with 4',6'-diamidino-2-phenylindole (DAPI). At least 30 grids were counted randomly for each slide for AO, FISH, and CARD-FISH counts. Probe hybridization details are given in Table 1. Cell numbers for conspicuous ANME-SRB aggregates were estimated using a semidirect method (7). All aggregates and cells were assumed to be spherical. The average cell volume was estimated to be 0.065 μm^3 . The volume of an average aggregate (82 μm^3) was divided by the cell volume, and a ratio of archaeal cells to bacterial cells of 1:1 was used to calculate bacterial and archaeal cell numbers in the consortium.

SEM-EDX. For scanning electron microscopy (SEM)-energy-dispersive X-ray (EDX) analysis, formalin-fixed samples were analyzed with a LEO 1550VP scanning electron microscope equipped with an in-lens detector, and element analysis was performed with an INCA Energy 300 system equipped with an Si(Li) detector.

16S rRNA gene construction and phylogenetic analysis. Sectioned sediment samples were frozen at -20°C until processing. Archaeal and bacterial 16S rRNA gene libraries were created as described by Niemann et al. (58). Briefly, total community DNA was extracted from sediment sections and orange flakes using a FastDNA spin kit for soil (Q-Biogene, Irvine, CA). Total DNA was extracted from formalin-preserved white granules using Chelex-100 resin. Granules were boiled at 100°C in the presence of Chelex-100 resin, the beads were allowed to settle, and the supernatant was used for PCR. The 16S rRNA gene was amplified from archaea using primers ARCH20F (49) and Uni1392R (38) and from bacteria using primers GM3F (53) and GM4R (31). Amplification products were cloned, and the purified plasmid was sequenced using an ABI 3100 genetic analyzer. Plasmids were sequenced initially in one direction (approx-

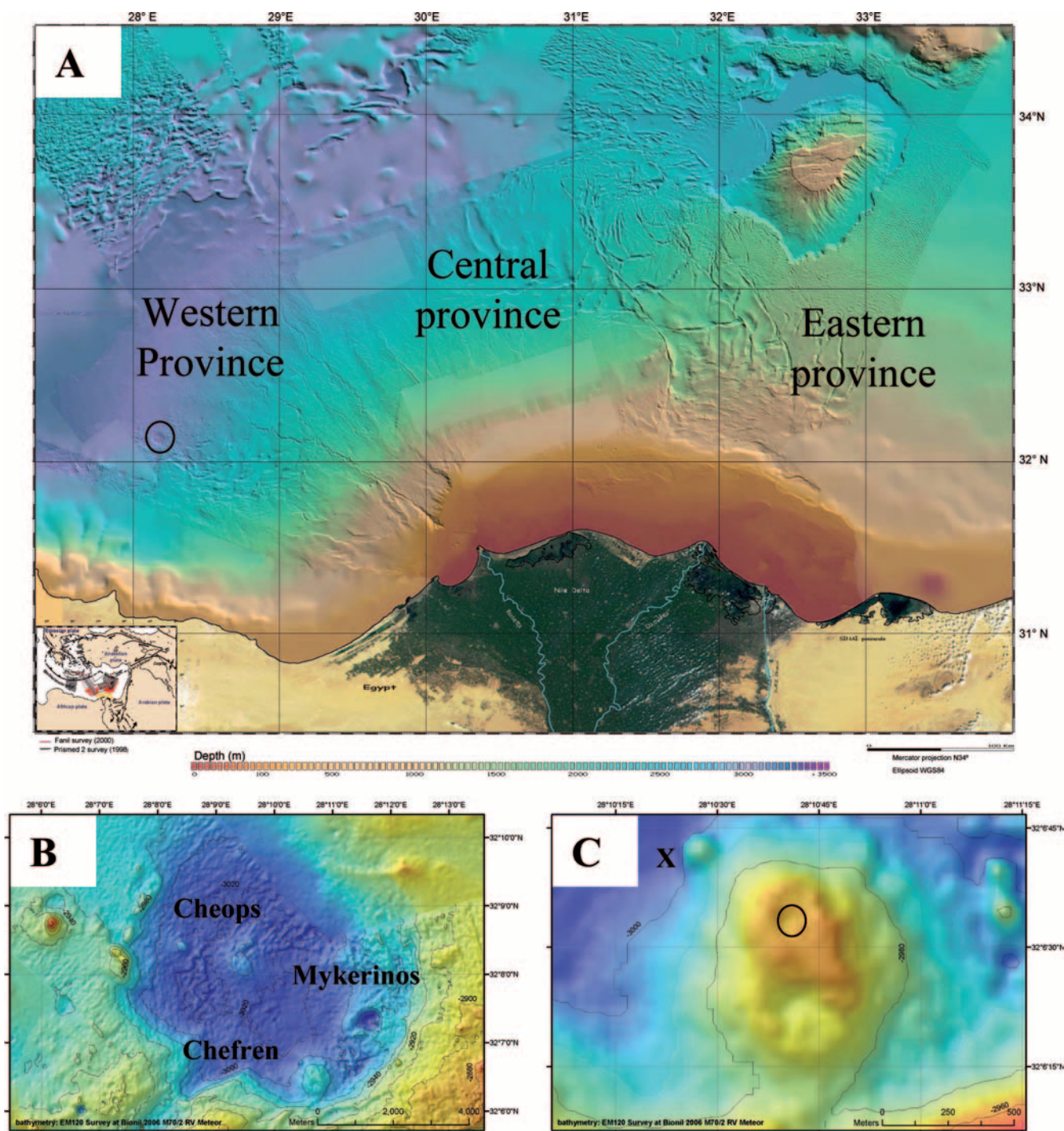


FIG. 1. (A) Bathymetric map of the Nile Deep Sea Fan. The circle indicates the position of the Menes Caldera. (Adapted from reference 47 with permission of Geosciences Azur/CIESM.) (B) Bathymetric map of the Menes Caldera with its three mud volcano systems. (C) Bathymetric map of the Chefren mud volcano. "X" indicates the location close to Chefren characterized by orange and white mats, and the circle indicates the location where brine samples were obtained during *Nautilie* dive 18. The maps in panels B and C were obtained during METEOR expedition BIONIL M70/2 in 2006 using the EM120 multibeam.

mately 0.6 kb). Sequences were manually inspected, and poor-quality sequences were removed from further analysis. Sequences were also screened for chimeras using the Mallard program (4). Anomalous sequences were then further investigated using BLAST and the Pintail program (3). Sequences with genuine chimeras were then excluded from further analyses. Selected clones were then sequenced fully (approximately 1.5 kb) and used for subsequent phylogenetic

analysis with the ARB (44) software package. Statistical analysis of 16S rRNA gene libraries was performed using the s-libshuff program by Schloss et al. (70). Distance matrices calculated with ARB using the neighbor-joining tool were used for s-libshuff.

Fluid flow models. Mass transfer models including fluid flow and molecular diffusion were created using the Comsol-Multiphysics modeling suite and were

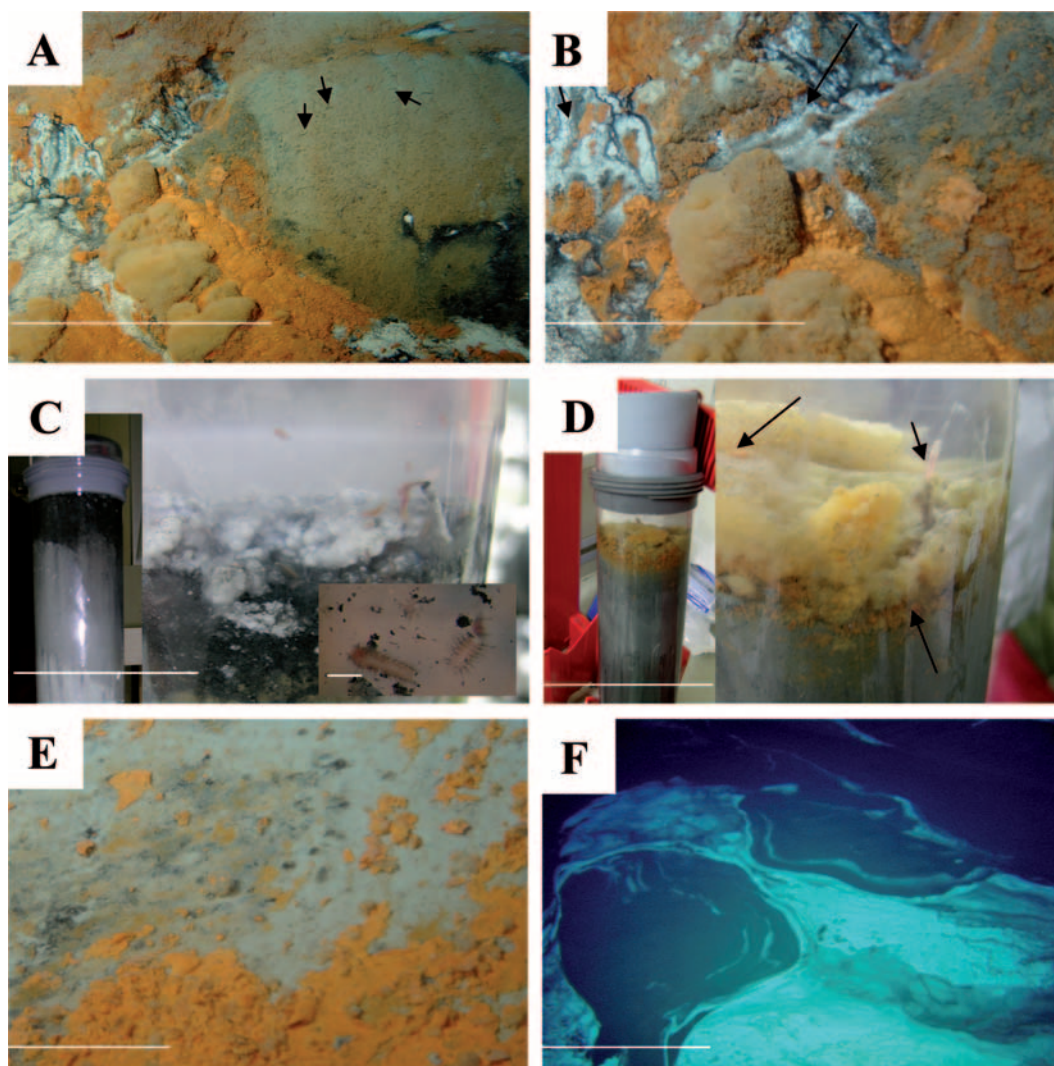


FIG. 2. Microbial mat system of the brine-impacted seep at the rim of the Chefren mud volcano. (A) Photograph taken by the submersible *Nautile* at the site of recovery of the orange and white mats. On the right side, the sediments are populated by sessile worms (arrows) forming tubes from sediment particles. Scale bar = 3 m. (B) Close-up of the mat system. Brine flowed downward (arrows) from the steep rim of the Chefren mud volcano across the white mats. Scale bar = 1 m. (C) Photographs of a core from the white mat. (Left) Black to gray sediment layers below the white mat. (Right) Top of the core. The white mat was composed of cotton ball-like precipitates overlying black fluidic sediments. Scale bar = 3 cm. (Inset) Small motile polychaetes associated with the white mat and the black sediment layer. The red color of the polychaetes indicates elevated hemoglobin levels, a typical adaptation to reduced sediments. Scale bar = 0.5 cm. (D) Photographs of a core from the orange mat. (Left) Greyish sediment layers below the orange mat. (Right) Top of the core. The arrows indicate a sessile worm (top arrows) and the orange fluffy material and flakes overlaying grayish sediments (bottom arrow). Scale bar = 3 cm. (E) Orange precipitates on sediments at the border of the brine lake. Scale bar = 20 cm. (F) Dense white mats floating on top of the large brine lake filling the center of the Chefren mud volcano. Scale bar = 3 m. (Panels A, B, E, and F were taken by the *Nautile* submersible during the 2003 Nautinil campaign [photos courtesy of Ifremer].)

calibrated against the measured Cl^- concentration. As Cl^- can be considered nonreactive, the mass balance is governed by diffusion and advection according to the following equation: $0 = \phi \cdot D_s \cdot d^2C/dz^2 - v\phi dC/dz$, where C is the pore water Cl^- concentration, z is the vertical distance, ϕ is the porosity, D_s is the diffusion coefficient for Cl^- in the pore space, and v is the vertical velocity.

Diffusion coefficients were corrected for tortuosity using the interpolated porosity at each depth and the procedure of Iversen and Jørgensen (25). The concentrations at the surface were set to the Cl^- concentration measured in the bottom water of the push cores, and the concentration at the lower boundary of the modeled regimen (1 m) was set to the concentration measured below 15 cm (below the white mat) or 17 cm (below the orange mat) in both cores. This left the pore water flow as the only unknown, which could be estimated by numerically finding the best fit to the measured Cl^- profiles. Each steady-state calcu-

lation was followed by 10 h of stagnation to include the time that the sediment was contained in the core liner before sectioning.

Nucleotide sequence accession numbers. Sequences determined in this study have been deposited in the GenBank database under accession numbers EF687138 to EF687656 and EF688595.

RESULTS

Visual observations. White mats and orange mats were located at a small brine seep on a steep slope at the bottom of a small mound adjoining the northwestern rim of the Chefren mud volcano (Fig. 1C) at a water depth of 3,020 m. The mats

TABLE 1. Oligonucleotide probes and hybridization conditions used in this study

Probe ^a	Target group	Sequence (5' to 3')	Type	Formamide concn (%)	Hybridization temp/wash temp (°C)	Reference
ARCH915	Most <i>Archaea</i>	GTGCTCCCCCGCCAATTCCT	CARD	35	46/48	2
ANME-1-350	ANME-1	AGTTTTTCGCGCCTGATGC	CARD	40	46/48	5
ANME-2-538	ANME-2	GGCTACCACTCGGGCCGC	FISH	50	46/48	82
ANME-3-1249	ANME-3	TCGGAGTAGGGACCCATT	CARD	20	46/48	41
EUB I	Most <i>Bacteria</i>	GCTGCCTCCCGTAGGAGT	CARD	35	46/48	2
EUB II	<i>Planctomycetales</i>	GCAGCCACCCGTAGGTGT	CARD	35	46/48	11
EUB III	<i>Verrucomicrobiales</i>	GCTGCCACCCGTAGGTGT	CARD	35	46/48	11
Non338	Negative hybridization probe	ACTCCTACGGGAGGCAGC	CARD-FISH	Variable	46/48	89
Alf968	<i>Alphaproteobacteria</i>	GGTAAGGTTCTGCGCGTT	FISH	35	46/48	55
Gam42	<i>Gammaproteobacteria</i>	GCCTTCCCACATCGTTT	FISH	35	46/48	46
Beta42a	<i>Betaproteobacteria</i>	GCCTTCCCACATCGTTT	FISH	35	46/48	46
DSS658	<i>Desulfosarcina/Desulfococcus</i>	TCCACTCCCTCTCCCAT	CARD	50	46/48	46
660	<i>Desulfobulbus</i>	GAATTCCACTTTCACCTCTG	CARD	60	46/48	13
Mγ705	Type I methanotrophs	CTGGTTCCTTCAGATC	FISH	20	46/48	15
Arc94	<i>Arcobacter</i>	TGCGCCACTTAGCTGACA	CARD	20	46/48	73

^a EUB-I, -II, and -III were mixed to obtain a single solution designated EUB I-III.

had a patchy distribution and covered about 25 m² (Fig. 2A and B). Shimmering brine fluid flowed downward from black sediments above the white mats (Fig. 2B). Associated with the orange patches at this site, and also at other areas of Chefren, were many crabs feeding on the sediments, which were populated by small worm tubes sticking out 1 to 2 cm above the sediment. The surfaces of the cores recovered from the white mat were composed of thick white cotton ball-like precipitates that resembled filamentous sulfur aggregates (Fig. 2C), which have previously been observed at hydrothermal vents (78). Polychaete larvae (Fig. 2C) were observed crawling through the white mats, as well as through the surface of the core. The surfaces of the cores from the orange mat were composed of a thick layer of fluffy yellow material, as well as flaky, bright orange particles, resembling Fe(III) (hydr)oxides (Fig. 2D). Similar to the cores from the white mat, polychaete larvae were also associated with the orange mat.

We followed the orange and white mat structure to the southwest along the same depth contour for about 50 m. Irregular patches of orange mat occurred within a band that was about 2 m wide and also in association with the edge of the brine lake in the center of the Chefren mud volcano (Fig. 2E). When using the manipulator arm of *Nautile* to dig into the orange patches, we observed that the subsurface sediments were dark gray to blackish, while the surrounding seafloor was light brown-beige, typical of pelagic sediments in the deep Eastern Mediterranean. No trace of gas ebullition was observed upon disturbance of the seafloor. Wide areas of the brine lakes located at the top of the Chefren and Cheops mud volcanoes were covered with white mats (Fig. 2F) similar to those observed on the sediments.

Microscopy. Examination of the granules recovered from the surface of the white mat (Fig. 3A) revealed the presence of tufts of thin filaments (Fig. 3B) morphologically similar to those produced by the epsilonproteobacterium "*Candidatus Arcobacter sulfidicus*" (77, 78). SEM coupled to EDX analysis revealed that these tufts were characterized by large amounts of Fe and S (Fig. 3C). Framboidal pyrite grains (not shown) were also detected within these granules. FISH with probe Arc94 (Fig. 3D), which targets "*Ca. Arcobacter sulfidicus*" and

related species, indicated that this group of organisms constituted up to 24% of the total cells within the white granules and in the underlying black sediment (Table 2). However, several morphologies (e.g., filamentous and coccoid) of cells which hybridized with the probe were observed, some of which were not the typical crescent-shaped "*Ca. Arcobacter sulfidicus*" cells.

Microscopic examination of flakes recovered from the surface of the orange mat (Fig. 2D and 3E) revealed numerous microbial sheaths of assorted sizes (Fig. 3F and G), similar to those produced by or attributed to the neutrophilic Fe(II)-oxidizing bacterium *Leptothrix ochracea* (16, 17, 86). EDX analysis revealed that many of these sheaths were associated with large amounts of Fe and O, indicating encrustation by Fe(III) (hydr)oxides. Most sheaths were sheared and empty (Fig. 3G). DAPI and AO staining both showed that very few sheaths (<1%) were populated with cells. FISH with the EUB I-III probe revealed that these sheaths contained bacteria, some of which could be targeted by the Mγ705 probe (Fig. 3H) for type I methanotrophs but not by domain-specific probes for *Alpha*-, *Beta*-, and *Gammaproteobacteria*. Two morphotypes of sheathed bacteria were targeted by the Mγ705 probe, one with rectangular cells similar to *Clonothrix fusca* cells (87) and the other with square cells similar to *Crenothrix polyspora* cells (75). These two morphotypes often appeared to be bundled together.

Fluid flow model. The orange mats had a shallow Cl⁻ gradient indicative of relatively low fluid flow. Hence, the 10-h stagnation of the flow in the core liners before processing had little effect on the shape of the profile, and the upward fluid flow velocity could be calculated with good accuracy and was 0.6 m per annum (a⁻¹) (Fig. 4B). The white mats were associated with a much steeper Cl⁻ gradient, indicating higher fluid flow velocities. The relaxation of the gradient during the 10-h recovery caused the maximum velocity to be uncertain, but the minimum upward fluid flow under the white mat was estimated to be 15 m a⁻¹ (Fig. 4A).

Biogeochemistry. Close to the white mat, the Cl⁻ and Na⁺ concentrations were up to 1.8 times higher than those in the bottom water (water overlying the sediment in the core), indi-

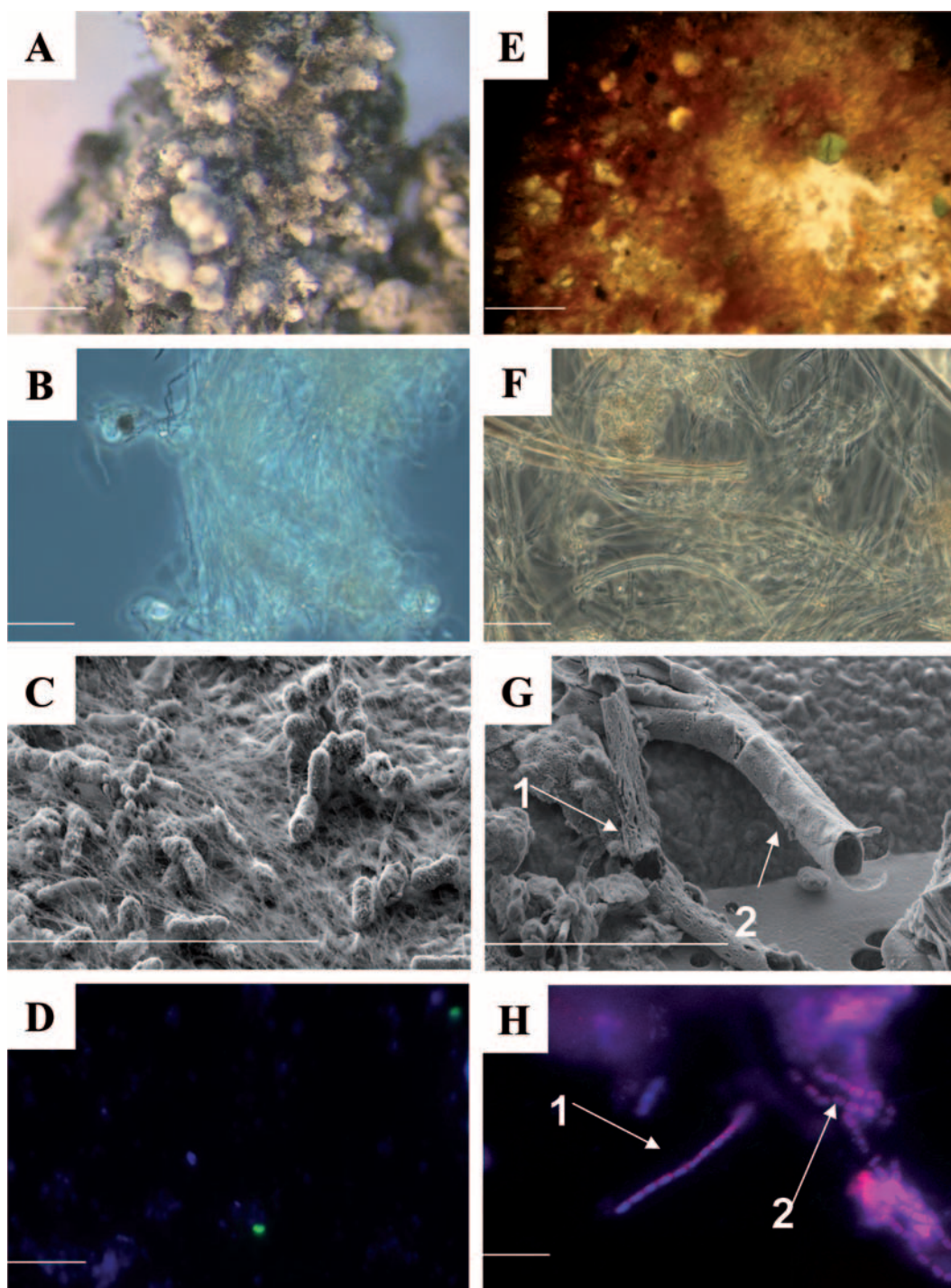


FIG. 3. (A) Dissecting microscope image of an S aggregate from the white mat. Scale bar = 1 mm. (B) Phase-contrast image of S filaments from the white mat. Scale bar = 10 μm . (C) High-resolution SEM image of filaments and associated cells from the white mat. (D) FISH image showing Arc94-targeted cells (green). (E) Image of Fe oxide flakes from the orange mat. Scale bar = 1 mm. (F) Light microscope image of an orange flake. (G) High-resolution SEM image of damaged sheaths from a flake. The arrows indicate two distinct types of sheathed bacteria (bacteria are not visible, but their sheaths are). (H) FISH image showing M γ 705-targeted sheaths. The arrows indicate two distinct types of sheathed bacteria similar to *C. fusca* (arrow 1) and *C. polyspora* (arrow 2). (B to D and F to H) Scale bars = 10 μm . Cores NL18PC3(5) and NL18PC1(8) were used for microscopy.

cating that there was upward brine flow through the sediments (Table 3). The pore water sulfate concentrations under the white mat (Fig. 5A) were close to seawater values at the surface and decreased to about 19 mM immediately below the

surface, possibly reflecting sulfate concentrations in the upwardly seeping fluids. The SR rates (Fig. 5A) were highest in the top 4 cm ($300 \text{ nmol} \cdot \text{cm}^{-3} \cdot \text{day}^{-1}$) and 70-fold higher than the AOM rates (Fig. 5B). The methane concentrations

TABLE 2. FISH counts for the white and orange mats, as well the underlying sediments^a

Core	Depth (cm)	ARC915			ANME-2			ANME-3			EUB I-III			DSS658			Arc94			Mfy705			
		Total no. of cells (10 ⁶)	No. of free cells (10 ⁶)	% of total cells	No. of free cells (10 ⁶)	% of aggregates	% of DAPL stained cells	No. of free cells (10 ⁶)	% of aggregates	% of total cells	No. of free cells (10 ⁶)	% of aggregates	% of total cells	No. of free cells (10 ⁶)	% of aggregates	% of total cells	No. of free cells (10 ⁶)	% of aggregates	% of total cells	No. of free cells (10 ⁶)	% of aggregates	% of total cells	
NL18PC(5) (white)	Mat	1.00	0.03	3	<	<	<	0.67	67	ND	0.24	24	ND	0.24	24	0.003	<	0.31	<	<	<	0.31	
	0-2	0.90	0.14	16	<	<	<	0.47	52	ND	0.20	23	ND	0.20	23	<	<	ND	<	<	<	ND	
	2-4	2.10	0.18	37	0.38	18	ND	0.49	51	ND	0.10	23	23	0.10	23	<	<	ND	<	<	<	ND	
	4-6	1.97	0.18	36	0.50	25	7	0.29	42	7	0.01	24	24	0.01	24	<	<	ND	<	<	<	ND	
	6-8	0.61	0.19	31	ND	ND	27	0.15	25	27	<	5	5	<	5	<	<	ND	<	<	<	ND	
	8-10	1.10	0.20	18	ND	ND	6	0.41	37	6	<	ND	ND	<	ND	<	<	ND	<	<	<	ND	
	10-12	0.42	0.07	18	ND	ND	ND	0.13	30	ND	<	ND	ND	<	ND	<	<	ND	<	<	<	ND	
	12-14	0.20	0.02	12	ND	ND	ND	0.12	60	ND	<	ND	ND	<	ND	<	<	ND	<	<	<	ND	
	14-16	0.20	0.03	14	ND	ND	ND	0.02	11	ND	<	ND	ND	<	ND	<	<	ND	<	<	<	ND	
	16-18	0.24	ND	ND	ND	ND	ND	ND	ND	ND	<	ND	ND	<	ND	<	<	ND	<	<	<	ND	
	NL18PC(8) (orange)	Mat	0.80	0.02	3	ND	ND	<	0.54	67	ND	0.03	10	10	0.03	10	<	<	8	<	<	<	8
		0-2	1.28	0.03	8	0.10	8	ND	0.78	66	ND	0.04	19	19	0.04	19	<	<	2	<	<	<	2
2-4		4.75	0.95	38	0.96	20	ND	1.09	41	ND	0.03	7	7	0.03	7	<	<	ND	<	<	<	ND	
4-6		0.76	0.19	25	ND	ND	25	0.27	36	ND	<	8	8	<	8	<	<	ND	<	<	<	ND	
6-8		1.15	0.25	22	ND	ND	22	0.30	26	ND	<	12	12	<	12	<	<	ND	<	<	<	ND	
8-10		1.09	0.16	14	ND	ND	14	0.38	35	ND	<	3	3	<	3	<	<	ND	<	<	<	ND	
10-12		0.91	0.24	26	ND	ND	26	0.16	17	7	<	10	10	<	10	<	<	ND	<	<	<	ND	
12-14		1.60	0.24	15	ND	ND	15	0.65	41	ND	<	12	12	<	12	<	<	ND	<	<	<	ND	
14-16		0.97	0.15	16	ND	ND	16	0.39	40	ND	<	11	11	<	11	<	<	ND	<	<	<	ND	
16-18		0.62	0.09	14	ND	ND	14	0.15	24	ND	<	ND	ND	<	ND	<	<	ND	<	<	<	ND	

^a The number of total cells is the number of cells obtained by AO direct counting. All cell numbers are per ml of sediment. The counts for the ANME-1 and 660 probes were both less than 1% of the total number of cells in all samples. "<" indicates that the number of cells was less than 0.1% of the total number of cells. ND, not determined.

(Fig. 5B) ranged from 0.1 mM at the top of the core to about 0.05 mM at the bottom. The AOM rates were low throughout the top 12 cm of sediment, with a maximum (10 nmol · cm⁻³ · day⁻¹) at a sediment depth of 2 to 4 cm (Fig. 5B). The sulfide concentrations (Fig. 5C) approached 1 mM in the zone with highest SR activity. Concurrently, Fe(II) (Fig. 5C) was depleted to a concentration of <0.01 mM at levels above 5 cm, but the concentration increased to about 0.2 mM below this zone. These gradients match visual characteristics of the core, namely, the precipitation of Fe(II) with sulfide in the black, highly reduced sediment horizon up to 6 cm below the white mat (Fig. 5D). In this layer, the Fe and S contents (Table 3) of the solid phase were several times higher than those in underlying sediments, indicating a high content of FeS and pyrite.

Below the orange mat, the sulfate concentration decreased from 28 mM at the surface to about 5 mM at a sediment depth of 8 cm (Fig. 5E). The Cl⁻ and Na⁺ concentrations indicated that the sediments were also brine impacted, although to a lesser extent than the sediment underneath the white mat (Table 3). The maximum SR rates (300 nmol · cm⁻³ · day⁻¹) (Fig. 5E) occurred at depths between 6 and 10 cm. This coincided with blackish, reduced sediment similar to that observed directly beneath the white mat. A second maximum SR rate (150 nmol · cm⁻³ · day⁻¹) was detected at 0 to 2 cm, just below the orange mat. The methane concentrations (Fig. 5F) under the orange mat ranged from less than 0.01 mM at the surface to about 0.1 mM at the bottom of the core (Fig. 5F). The AOM rates were highest in the first few centimeters (13 nmol · cm⁻³ · day⁻¹). The SR rates in these sediments also exceeded the AOM rates by 11-fold. The sulfide concentrations under the orange mat were less than 0.01 mM. In contrast, the Fe(II) concentrations decreased from 0.7 mM just below the sediment surface to zero below a sediment depth of 16 cm (Fig. 5G). Fe(II) was completely consumed in the surface layer below the orange mat. The solid-phase Fe and S contents (Table 3) were high throughout the core, but the Fe level was elevated in the orange mat and in the 5- to 7-cm zone. In view of the Fe content and the much lower S content, it is likely that both horizons contained substantial amounts of Fe oxides.

The organic carbon contents (Table 3) in both cores were low (0.18 to 0.77%), which is typical for oligotrophic Eastern Mediterranean deep-sea sediments, indicating that the energy source for microbial reactions was not detritus based.

CARD-FISH and FISH counts. The total cell numbers (Table 2) for both cores were around 10⁹ cells · cm⁻³ in the upper 10 cm. In the white mat and its underlying sediment, the total cell numbers decreased to 10⁸ cells · cm⁻³ below 10 cm, whereas below the orange mat the total cell numbers were more or less stable for the first 18 cm of sediment. Archaeal cells accounted for less than 3% of the total cells in both mats but generally accounted for 12 to 38% of the total cells in the underlying sediments. In accordance with the biogeochemistry of the cores, ANME were detected in the top 6 cm of both cores (Table 2 and Fig. 6A and C). ANME-2 cells formed consortia with SRB belonging to the *Desulfosarcina/Desulfococcus* cluster (Fig. 6A). Free-living ANME-2 cells were not detected in the sediments. In contrast, the ANME-3 cells were all single cells and comprised 6 to 27% of the total cells in

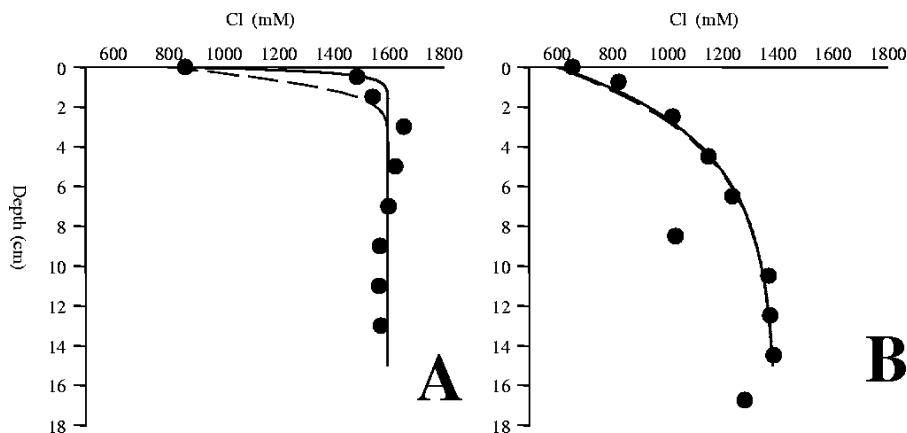


FIG. 4. Cl^- profiles from fluid flow models. (A) Measured Cl^- profile from underneath the white mats (circles), modeled Cl^- profile at a constant flow of $15 \text{ m} \cdot \text{a}^{-1}$ (straight line), and modeled Cl^- profile after 10 h with a fluid flow velocity of zero (dashed line). (B) Measured Cl^- profile from underneath the orange mats (circles), modeled Cl^- profile at a constant flow of $0.6 \text{ m} \cdot \text{a}^{-1}$ (straight line), and modeled Cl^- profile after 10 h with a fluid flow velocity of zero (dashed line).

the 6- to 10-cm zone under the white mat and 7% of the total cells in the 8- to 12-cm zone under the orange mat (Table 2 and Fig. 6B).

The mats, as well as the top 2 cm of sediment from both cores, were dominated by bacteria (52 to 67% of the total cells in the sediments [Table 2]). DSS658-targeted SRB made up less than 1% of the white mat community (Table 2 and Fig. 6C). The level increased to 5 to 25% of the total cells in the top 6 cm of sediment underneath the mat, where the maximum SR rate was detected, and dropped again to <1% in deeper sediment. DSS658-targeted SRB were more abundant in the orange mat and underlying sediment, where they comprised 8 to 19% of the total cells.

Arc94-targeted cells made up 5 to 24% of the white mat and

the top 4 cm of the underlying sediment (Table 2 and Fig. 3D). These cells comprised 4% of the total cells within the orange mat and <1% of the total cells in the underlying sediment. Type I methanotrophs targeted by M γ 705 (Table 2 and Fig. 3H) comprised <1% of the cells in the white mat and in the sediment but 2 to 8% of the cells in the orange mat and the 2-cm interval beneath it.

16 rRNA gene analyses. 16S rRNA gene libraries for bacteria were constructed for both mats and the top 4 cm of sediment beneath the mats, whereas archaeal libraries were constructed only for the sediments. The phylotypes identified in the bacterial libraries for the mats, as well as for the underlying sediment, were very diverse and corresponded to microorganisms capable of many types of C, Fe, N, O, and S transforma-

TABLE 3. Pore water and solid-phase geochemical profiles of the white and orange mats, as well as the underlying sediments

Mat	Depth (cm)	Organic C (%, wt/wt)	Cl (mM)	Na (mM)	Fe (%, wt/wt)	S (%, wt/wt) ^a
NL18PC(6) (white)	Bottom water		863	704		
	0–2		1,487	1,240	13.6	11.35
	2–4	0.70	1,545	1,209	17.14	15.54
	4–6	0.44	1,657	1,282	5.10	2.10
	6–8	0.77	1,627	1,317	13.87	12.47
	8–10	0.24	1,602	1,317	3.50	<
	10–12	0.23	1,571	1,293	5.00	<
	12–14	0.22	1,567	1,244	4.85	<
	14–16	0.21	1,573	1,332	5.23	<
	16–18	0.18		1,380	2.51	<
18–20	0.21		1,301	2.17	<	
VL18PC(7) (orange)	Bottom water		657	565		
	Mat				11.62	3.51
	0.75	0.60	824	737	5.08	2.37
	1–3	0.53	1,020	913	4.34	1.80
	3–5	0.44	1,151	1,011	4.32	1.45
	5–7	0.61	1,239	1,099	7.77	1.19
	7–9	0.56	1,031	871	4.88	2.03
	9–11	0.57	1,370	1,187	5.06	2.46
	11–13	0.58	1,375	1,235	5.19	2.50
	13–15	0.56	1,388	1,242	4.84	2.04
15–17			1,153			

^a <, below detection.

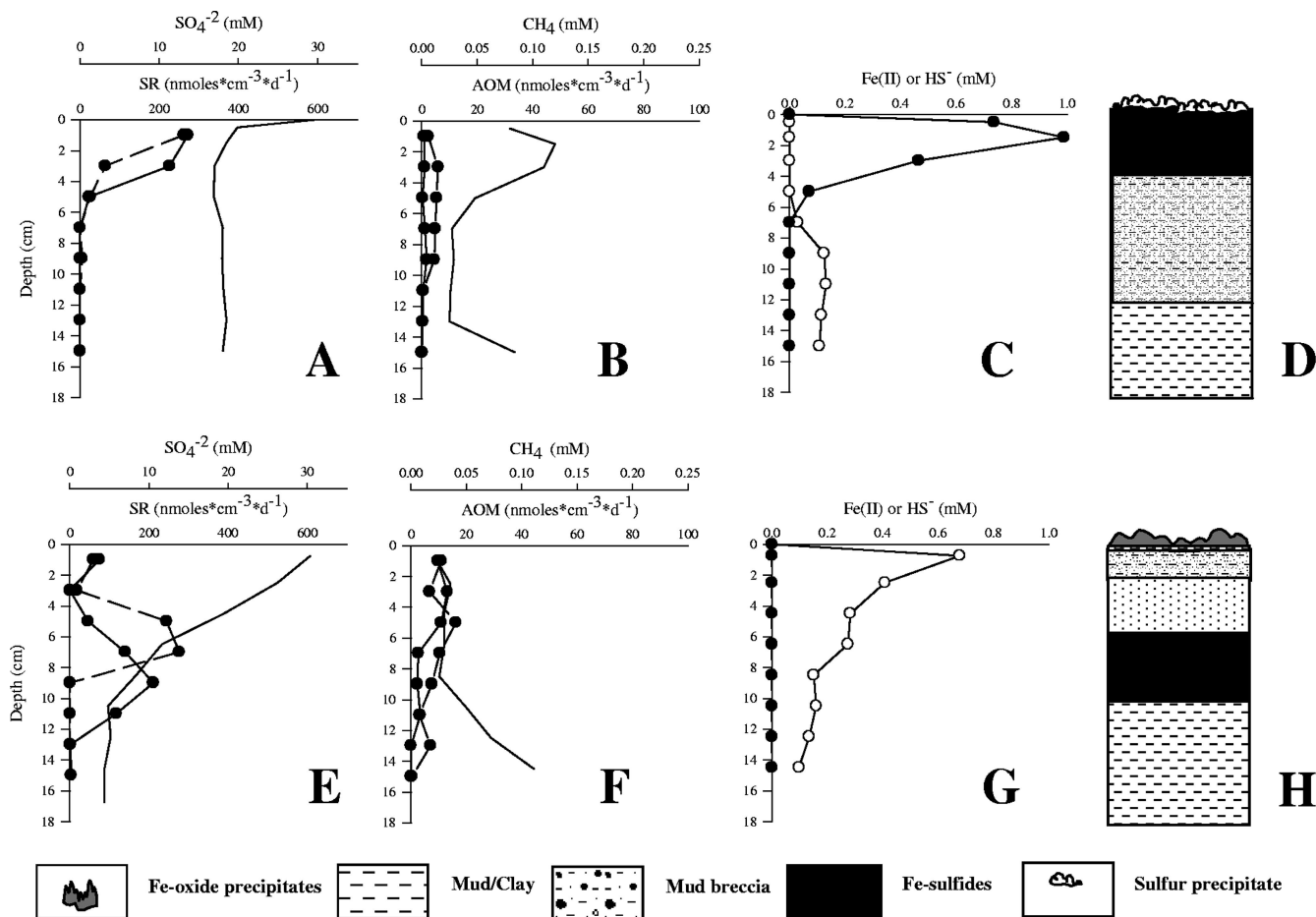


FIG. 5. (A) Replicate SR rates (circles) and sulfate concentrations underneath the white mats. (B) Replicate rates of methane oxidation (circles) and methane concentrations underneath the white mats. (C) Fe(II) (open circles) and HS^- (filled circles) concentrations underneath the white mats. (D) Sedimentological description of the sediment underneath the white mats. (E) Replicate SR rates (circles) and sulfate concentrations underneath the orange mats. (F) Replicate methane oxidation rates (circles) and methane concentrations underneath the orange mats. (G) Fe(II) (open circles) and HS^- (filled circles) concentrations underneath the orange mats. (H) Sedimentological description of the sediment underneath the orange mats.

tions. The *Deltaproteobacteria* represented the largest group of sequences in all of the libraries except those for the orange mat (Table 4 and Fig. 7). Most of these sequences were closely related to sequences of the *Desulfobacteraceae* and *Desulfobulbaceae* SRB clades. Sequences belonging to relatives of the *Desulfuromonadaceae* were recovered from the sediments underneath the orange mat, as well as from the white mat (Table 4 and Fig. 7). Members of this family are capable of Fe(III) and S reduction (42, 66).

The *Gammaproteobacteria* sequences were the largest group of bacterial sequences (74 to 34%) from the orange mat and a major group of sequences in the sediment underneath this mat (Table 4 and Fig. 8). Most of these sequences belonged to type I methanotrophs (42 to 7%), and the most closely related cultivated isolates (<91% identity) were *Methylobacter marinus*, *C. polyspora*, *C. fusca*, and other isolates. Sequences most closely related (>95% identity) to "*Ca. Arcobacter sulfidicus*" and *Sulfurimonas autotrophica* made up 32% of the sequences recovered from the white mat. Sequences closely related to

sequences from *Sulfurospirillum arcachonense* (>95% identity) were also recovered from both mats.

Sequences from ANME-2a, ANME-2c, and ANME-3 accounted for 55 to 74% of the archaeal sequences from the sediment below the white and orange mats (Table 4 and Fig. 9). ANME-3 sequences were detected only under the white mat and not under the orange mat, although ANME-3 cells were detected by FISH in both sediments. The ubiquitous seep- and subsurface sediment-associated groups of *Crenarchaeota* and *Euryarchaeota*, MBGB and MBGD, respectively, accounted for significant portions (19 to 38%) of the sequences recovered from the sediment of both cores.

DISCUSSION

Primary productivity and organic matter fluxes to the seafloor have varied greatly in the history of the Eastern Mediterranean Sea, but today this body of water is one of the most oligotrophic seas. Its bottom waters are fully oxygenated, and

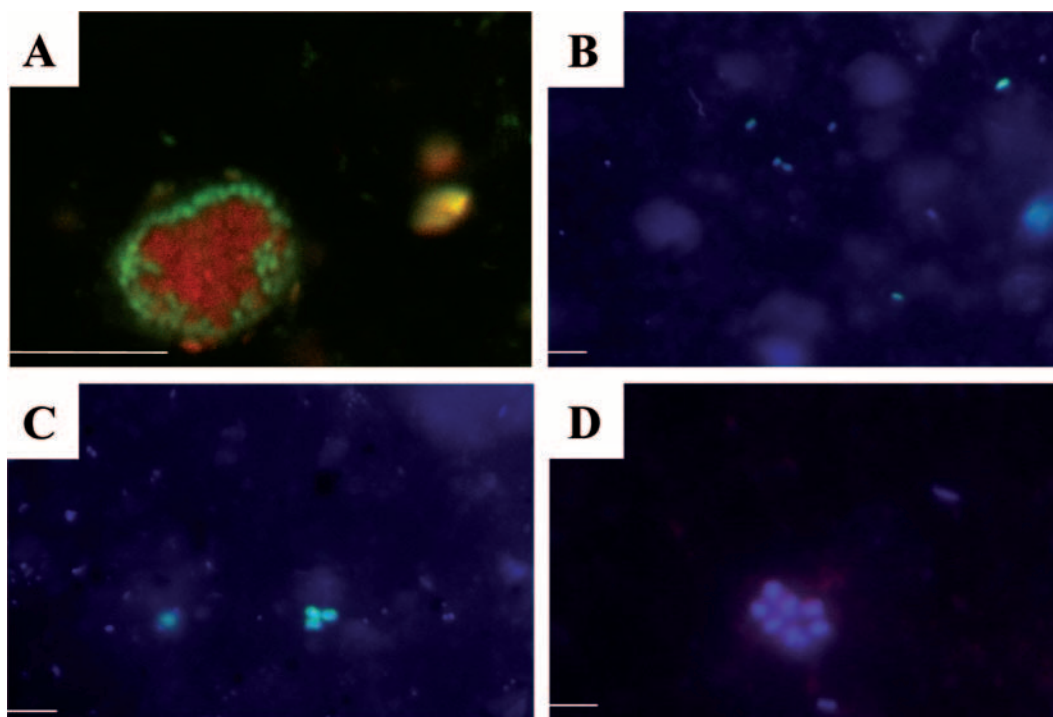


FIG. 6. (A) Double hybridization using FISH probes ANME2-538 (red) and DSS658 (green). (B) ANME3-1249-targeted cells. (C) DSS658-targeted cells. (D) My705-targeted single cells. Bars = 10 μm . Cores NL18PC3(5) and NL18PC1(8) were used for microscopy.

the organic matter flux to the seafloor is very low (8, 37, 60). Surface-exposed reduced sediments and accumulations of organisms, such as sulfide-oxidizing bacteria, tubeworms, and bivalves (Fig. 2 and 3), are clear indications of seepage of energy-rich compounds, such as methane, higher hydrocarbons, and sulfide. Living cold seep communities and biogeochemically active, fluid flow-impacted sediments have been found along the Eastern Mediterranean Ridge system (62) and the Nile Deep Sea Fan (14; G. Bayon, L. Loncke, S. Dupré, J.-C. Caprais, E. Ducassou, S. Duperron, J.-P. Foucher, Y. Fouquet, S. Gontharet, G. M. Henderson, J. Etoubleau, I. Klauke, J. Mascle, S. Migeon, H. Ondréas, C. Pierre, C. Huguen, A. Stadnitskaia, J. Woodside, and M. Sibuet, submitted for publication; Omeregine et al., submitted).

Generally, at cold seeps, sites with high sulfide fluxes across the seafloor are marked by mat-forming bacteria, which oxidize sulfide to sulfur or sulfate, using oxygen or nitrate as the electron acceptor. The cells are often mobile and hence can bridge the gap between sulfide and oxygen penetration in the sediments. The giant vacuolated sulfide oxidizers store elemental sulfur internally, which gives the mats a characteristic white color (29, 56, 61). Mats formed by giant vacuolated sulfide oxidizers typically appear to be smooth (59), furry (attached vacuolated filamentous cells) (61), or crusty (e.g., *Thiomargarita* spp. cold seep mats [29]). The mats described here have a different appearance both macroscopically (cotton ball structure) and microscopically (external sulfur storage).

To our knowledge, orange mats have not been described previously for marine cold seeps, but similar mats have been found in a few hydrothermal vent settings (16, 34, 74) and at groundwater Fe(II) seeps (17). At these sites, the mats are

thought to be created by Fe(II)-oxidizing *Beta*- or *Gammaproteobacteria* belonging to the genera *Gallionella*, *Leptothrix*, and *Marinobacter*, as well as the gammaproteobacterial strain PV-1. Both the orange and white mats investigated here appear to represent important communities at brine-impacted cold seeps of the Eastern Mediterranean and were commonly observed floating on the brine (white mats [Fig. 2F]) or at the edge of brine lakes (orange mats [Fig. 2E]).

Composition of the white mats and orange mats. The granules recovered from the white mat were composed of elemental S filaments, as shown by light microscopy, SEM, and EDX analysis (Fig. 3). These filaments were most likely produced by chemoautotrophic sulfide-oxidizing organisms related to “*Ca. Arcobacter sulfidicus*,” as indicated by 16S rRNA gene analysis and FISH, which showed that up to 24% of the cells within the mat were cells of close relatives of this organism. “*Ca. Arcobacter sulfidicus*” secretes long S filaments as a by-product of sulfide oxidation (72), forming dense accumulations of elemental S in hydrothermal vent settings (72) and in laboratory bioreactors (77). “*Ca. Arcobacter sulfidicus*” has also been detected in cold seep settings (65). These environments are typically sulfidic, high-fluid-flow environments where sulfide and oxygen gradients overlap due to advective processes.

Sequences closely related to sequences of *Desulfocapsa sulfofexigens*, which is capable of S disproportionation into sulfide, sulfate, and H^+ (19), represented another significant portion of the sequences from the white mat. The activities of these organisms within this mat would likely enhance S cycling as they would consume S, as well as provide additional sulfide.

The flakes that made up the orange mat were composed of Fe(III) (hydr)oxide-encrusted sheaths (Fig. 3F and G) similar

TABLE 4. Breakdown of 16S rRNA gene sequence groups, expressed as percentages obtained from the white and orange mats as well as the top 4 cm of sediment beneath the mats

Location	Total no.	Bacterial clones									
		% <i>Alphaproteobacteria</i>	% <i>Gammaproteobacteria</i>	% Type I methanotrophs	% <i>Deltaproteobacteria</i>	% <i>Desulfobacteraceae</i> (% <i>Desulfosarcina variabilis</i>)	% <i>Desulfobulbaceae</i> (% <i>Desulfocapsa sulfexigens</i>)	% <i>Desulfurimonadaceae</i>	% <i>Epsilonproteobacteria</i>	% " <i>Ca. Arcobacter sulfidicus</i> "	% <i>Sulfurospirillum arcachonense</i>
White mat	91	1	2	0	32	2 (0)	20 (20)	9	36	2	2
White mat sediment	83	0	8	2	42	30 (23)	8 (6)	0	0	0	0
Orange mat	120	3	74	42	7	1 (0)	6 (0)	0	12	1	0
Orange mat sediment	88	1	34	7	31	16 (10)	10 (1)	1	7	0	0

to those produced by the neutrophilic Fe(II)-oxidizing beta-proteobacterium *L. ochracea* (86). Such sheaths have been shown to be encrusted with Fe(III) (hydr)oxides (33, 74) and were identified in several hydrothermal vent settings (16, 34, 74). The metabolism of *L. ochracea* is unclear as this species has not been obtained in pure culture. However, *L. ochracea* is generally considered a heterotroph and is often found in organic matter-rich environments. It is unlikely that the low organic carbon content of the Chefren sediments provides energy to heterotrophic mat-forming iron oxidizers (Table 3). Hence, we speculate that the organisms responsible for mat formation are unknown chemoautotrophs, which obtain energy from aerobic Fe(II) oxidation utilizing the high flux of upwardly flowing, Fe(II)-rich pore water.

Fe(II)-oxidizing bacteria are thought to form Fe oxide-encrusted sheaths in order to locate the electron transfer process close to the cell, as well as provide a means for the cell to escape encrustation by Fe(III) (hydr)oxides. The energetic yield of this process is very low; therefore, large amounts of Fe(II) need to be turned over in order to provide enough energy for growth, leading to large amounts of Fe(III) (hydr)oxide but very few cells (16). Neutrophilic Fe(II) oxidation, although it occurs in a variety of environments, such as hydrothermal vents (16), freshwater springs (26), and plant root nodules (18), remains somewhat enigmatic, as under these conditions Fe(II) spontaneously oxidizes to Fe(III). However, neutrophilic Fe(II)-oxidizing bacteria have been shown to increase Fe oxidation rates to values that are up to fourfold greater than abiotic rates (26, 57). The exact mechanism of this process is currently unknown, but it has been suggested that it occurs through the binding and sequestration of Fe(II) by bacterial exopolymers (57).

It is possible that the M γ 705-targeted sheaths and related 16S rRNA gene sequences obtained from the orange mat corresponded to organisms similar to *C. polyspora* and *C. fusca* (87). They often occur bundled together, as observed in this study. Whether these organisms can oxidize Fe(II) in addition to methane remains unclear, as they have only recently been cultivated. However, they are often found in environments where Fe(II) and methane cooccur, such as groundwater springs. Additionally, there have been several reports of *C. polyspora* sheaths incrusting in Fe(III) (hydr)oxides (79, 88). No 16S rRNA gene sequences recovered from the orange mat were similar to sequences of known Fe(II)-oxidizing species

(e.g., sheath-forming *Leptothrix* spp., stalk-forming *Gallionella* spp., PV-1, and other organisms).

In contrast, the orange mat contained many 16S rRNA gene sequences from bacteria that may constitute the reductive portion of the Fe cycle. Interestingly, sequences that grouped with *Sulfurospirillum deleyianum*, which is capable of Fe(III) reduction via S cycling, were detected within this mat (76). The presence of an active group of such microorganisms could couple and enhance S and Fe cycling by oxidizing S compounds with Fe(III). Additionally, enrichments (Straub et al., unpublished) using sediment from underneath the white mat with ferrihydrite as the sole electron acceptor resulted in high numbers of "*Ca. Arcobacter sulfidicus*" sequences in the 16S rRNA gene libraries, suggesting that these organisms have a role in Fe(III) reduction.

Biogeochemical processes supporting white and orange microbial mat formation. Spatial heterogeneity in fluid flow on scales of meters to kilometers has been observed in several cold seep systems (45, 67). Here we observed large variations in fluid flow (Fig. 4) through microbial mats on scales of centimeters to meters associated with brine seepage. Brine seepage is a common feature of mud volcanoes in the Eastern Mediterranean Ridge (90, 91) and western province of the Nile Deep Sea Fan (Huguenot et al., submitted). The brines often comigrate with hydrocarbons and sulfides (12, 84). Fluids from the brine pool at Chefren had high methane (2.4 mM) and sulfide (7.2 mM) concentrations, a salinity of 150‰, and sulfate concentrations of around 50 mM (J.-C. Caprais, personal communication). Unfortunately, we could not sample the brine flowing from black exposed sediments to the white mats (Fig. 2B), but it is likely that sulfide was present in the brine, which precipitated Fe(II). The brine flow across the white mat likely impeded the exchange with oxygenated water from the water column, providing a microaerophilic environment for sulfide oxidation. Although the Cl⁻ and Na⁺ profiles indicated that there was upward fluid flow, the possibility of multidirectional (i.e., lateral and downward) advection cannot be ruled out.

Sulfide underneath the white mat was clearly provided by SR rather than by upward transport with brine (Fig. 5). Furthermore, the distribution of DSS658-targeted cells matched the sulfide profile, as these cells accounted for a maximum of 24% of the total cells between 0 and 6 cm (Table 2). Although our sampling resolution did not allow precise determination of the limits of sulfide penetration, the rapid sulfide consumption at

TABLE 4—Continued

Bacterial clones				Archaeal clones								
% <i>Sulfurimonas</i> <i>autotrophica</i>	% Other bacteria	% Unidentified bacteria	Total no.	% <i>Euryar-</i> <i>chaeota</i>	% Possible ANME	% ANME- 2A	% ANME- 2C	% ANME- 3	% MBGD	% Unidenti- fied <i>Euryar-</i> <i>chaeota</i>	% <i>Crenar-</i> <i>chaeota</i>	% MBGB
30	29	0	71	96	0	18	1	55	15	6	4	4
0	42	7										
0	5	0	66	98	3	52	3	0	36	4	2	2
0	22	6										

the fluidic top of the core was likely due to the activity of “*Ca. Arcobacter sulfidicus*” and other sulfide oxidizers. This environment is similar to high-fluid-flow environments (72, 77), where sulfide and oxygen overlap due to advective processes, and is likely to be a niche for “*Ca. Arcobacter sulfidicus*” rather than for the giant vacuolated sulfide-oxidizing bacteria.

Similar to the biogeochemistry of the white mat, the SR rates under the orange mat were significantly higher than the AOM rates (Fig. 5). SRB cells accounted for 7 to 19% of the total cells under the orange mat. The maximum SR activity occurred at roughly 4 to 10 cm, which corresponded to the zone where there were increased amounts of solid-phase Fe and S (Fig. 5). Sulfide produced in this subsurface zone likely caused the precipitation of Fe and S complexes, similar to the situation in the sediment horizon directly under the white mat. No free sulfide was detected within this core; therefore, it is likely that the entire sulfide production went into the reduction of Fe(III) and precipitation of Fe(II). The source of the very high free Fe(II) concentration under the orange mat remains unknown; in situ microbial Fe(III) reduction and upward flow of Fe-rich subsurface fluids are plausible possibilities.

Bacterial community composition. As predicted from the markedly different biogeochemistries, significant differences (P value of < 0.01) were detected in comparisons of bacterial 16S rRNA gene libraries obtained in this study between the two mats, as well as between the mats and their underlying sediments. The importance of SR was reflected by the high percentage of sequences (Table 4) belonging to members of the *Deltaproteobacteria* in both sediment libraries (31 to 42% [Table 4]). As expected, these sequences grouped with sequences from genera of known sulfate reducers (Fig. 7) present at cold seeps, such as *Desulfobacter*, *Desulfosarcina*, *Desulfocapsa*, and *Desulfobulbus* (35). Some members of these genera are also capable of iron reduction (43), which occurred within the orange mat and in the underlying sediment. Sequences from members of the *Gammaproteobacteria* which are able to perform Fe(II) oxidation, sulfide oxidation, or methane oxidation were very prevalent in the libraries (8 to 74%). Most of these organisms grouped with aerobic type I methanotrophs, such as *M. marinus*, *C. polyspora*, and *C. fusca* (Fig. 8), as well as with environmental sequences from methane-rich sediments and symbionts in the gills of methanotrophic clams. Cultivated members of this group primarily oxidize methane with oxygen, but they are also capable of oxidizing other C-1 compounds. As

methane occurred at the top of both cores and was present in the water column, the sediment surface and especially the more oxidized orange mats represent potential niches for aerobic methanotrophy.

The high numbers of sequences of sulfur-oxidizing *Epsilonproteobacteria* (Fig. 8) in the white mat are consistent with the visual and biogeochemical data.

Archaeal community composition. Fifty-five to 74% of the archaeal sequences (Table 4) recovered from sediments underlying the orange and white mats belonged to the ANME-2 and ANME-3 clusters (Fig. 9). The quantitative distributions of these sequences differed between the sediments underlying the mats, and they overlapped only in one horizon (4 to 6 cm) under the white mat (Tab 3). In contrast, most other cold seeps typically contain a mixture of ANME communities and there is a clear dominance of one community (36). The Chefred seep represents the second known cold seep habitat characterized by a relatively high abundance of ANME-3 cells (59). However, none of the ANME-3 cells that were detected were associated with bacterial partners. The remaining archaeal sequences comprised members of two marine benthic groups (MBGB and MBGD) which are typical members of cold seep and subsurface communities (22, 36). However, no members of these two groups have been cultivated; therefore, their roles in the sediments of Chefred and elsewhere remain unknown. A comparison of the coverage of archaeal sequences from sediments underneath the white mat to the coverage of archaeal sequences from sediments underneath the orange mat revealed a statistical difference (P value of < 0.01), indicating a different community structure. The reciprocal test showed that the sediment community under the orange mat was not significantly different from that under the white mat (P value of > 0.05); rather, it may have represented a subset of the white mat community. It is possible that the archaeal communities were more similar to each other than to the bacterial community in the sediments because they were largely comprised of methanotrophs, which could be less affected by the differences in sulfide and iron biogeochemistry.

Comparison to other cold seep ecosystems. While the fluid flow velocities and SR rates were similar to those in previously investigated cold seep systems, the associated AOM rates were comparatively low (58, 59, 81, 83; Omoregie et al., submitted). The ratio of the SR rate to the methane oxidation rate ($>28:1$) differed substantially from the known stoichiometry of AOM

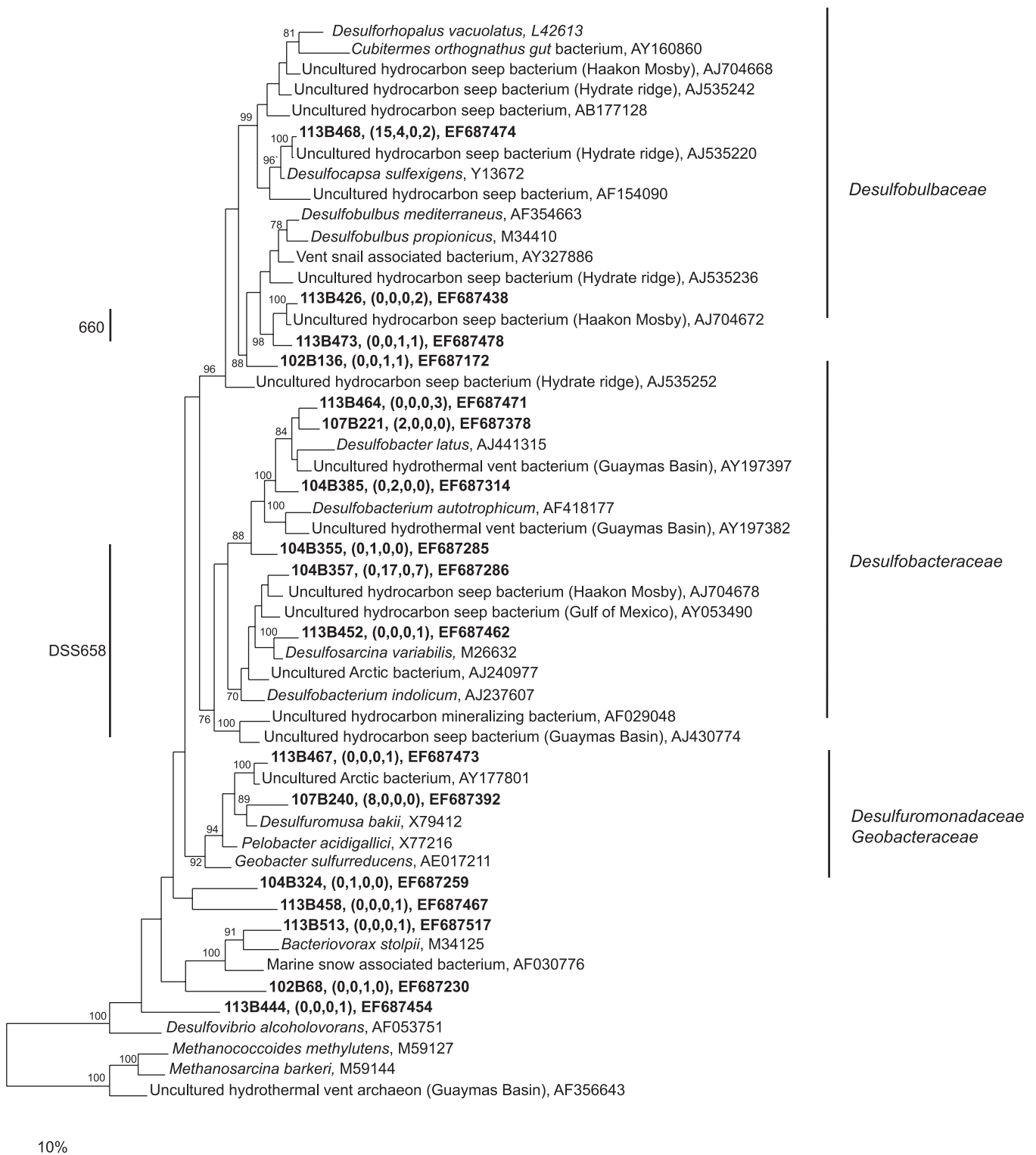
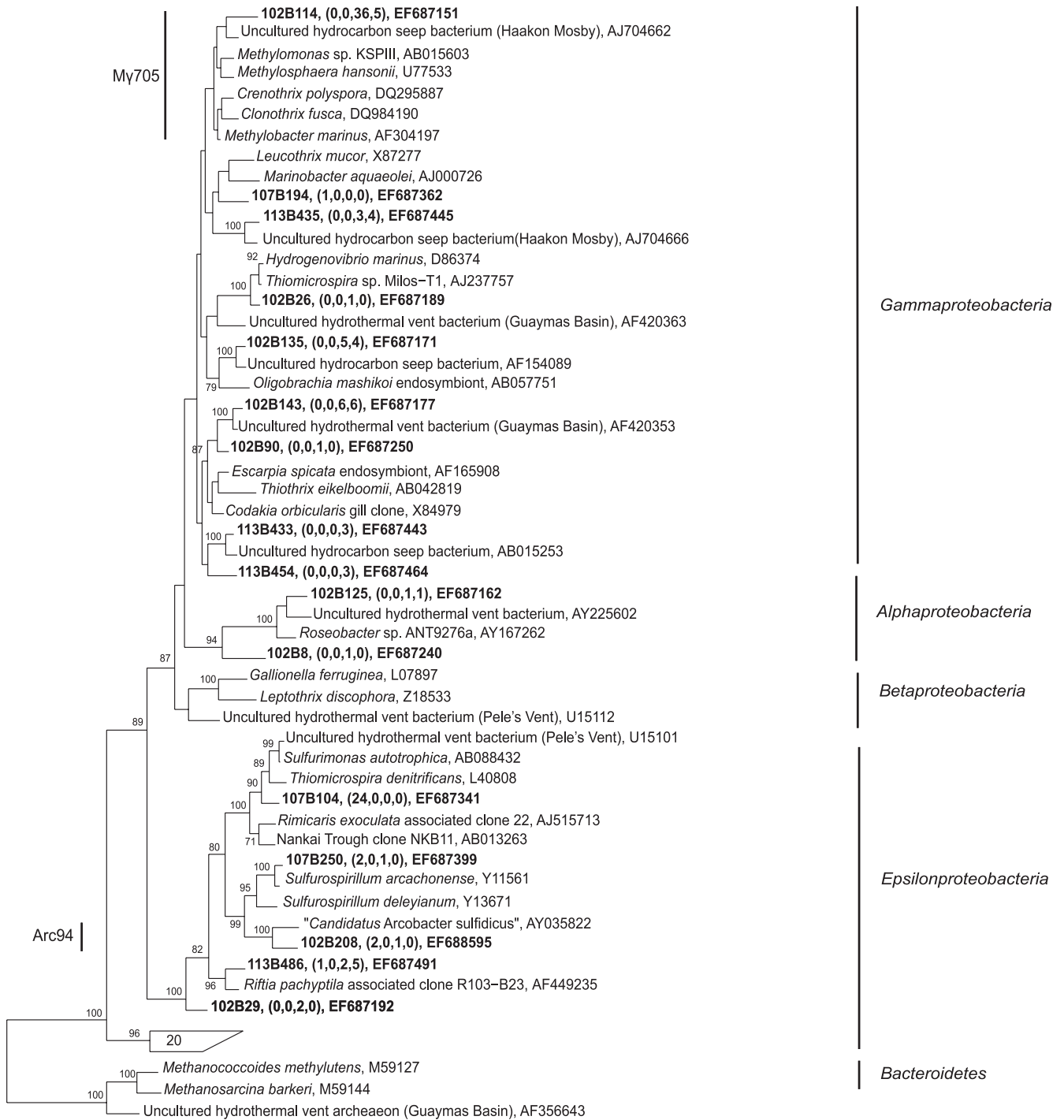


FIG. 7. Maximum parsimony tree of 16S rRNA gene sequences from *Deltaproteobacteria* obtained in this study, as well as from the GenBank database. The names in brackets are those of well-known cold seeps and hydrothermal vents. The bootstrap values at the nodes are percentages based on 500 replicates. Sequences obtained in this study are indicated by bold type, and the numbers in parentheses indicate the numbers of sequences with 98% identity to the relevant sequences from the white mat, the sediment underlying the white mat, the orange mat, and the sediment underlying the orange mat. Only selected sequences are displayed. Sequences that are targeted by the DSS658 and 660 probes are indicated.



10%

FIG. 8. Maximum parsimony tree of 16S rRNA gene sequences from *Gamma*-, *Beta*-, and *Epsilonproteobacteria* and unidentified sequences obtained in this study, as well as from the GenBank database. The bootstrap values at the nodes are percentages based on 500 replicates. The names in brackets are those of well-known cold seeps and hydrothermal vents. Sequences from this study are indicated by bold type, and the numbers in parentheses indicate the numbers of sequences with 98% identity to the relevant sequences from the white mat, the sediment underlying the white mat, the orange mat, and the sediment underlying the orange mat. Only selected sequences are displayed. Sequences that are targeted by Arc94 and My705 are indicated.

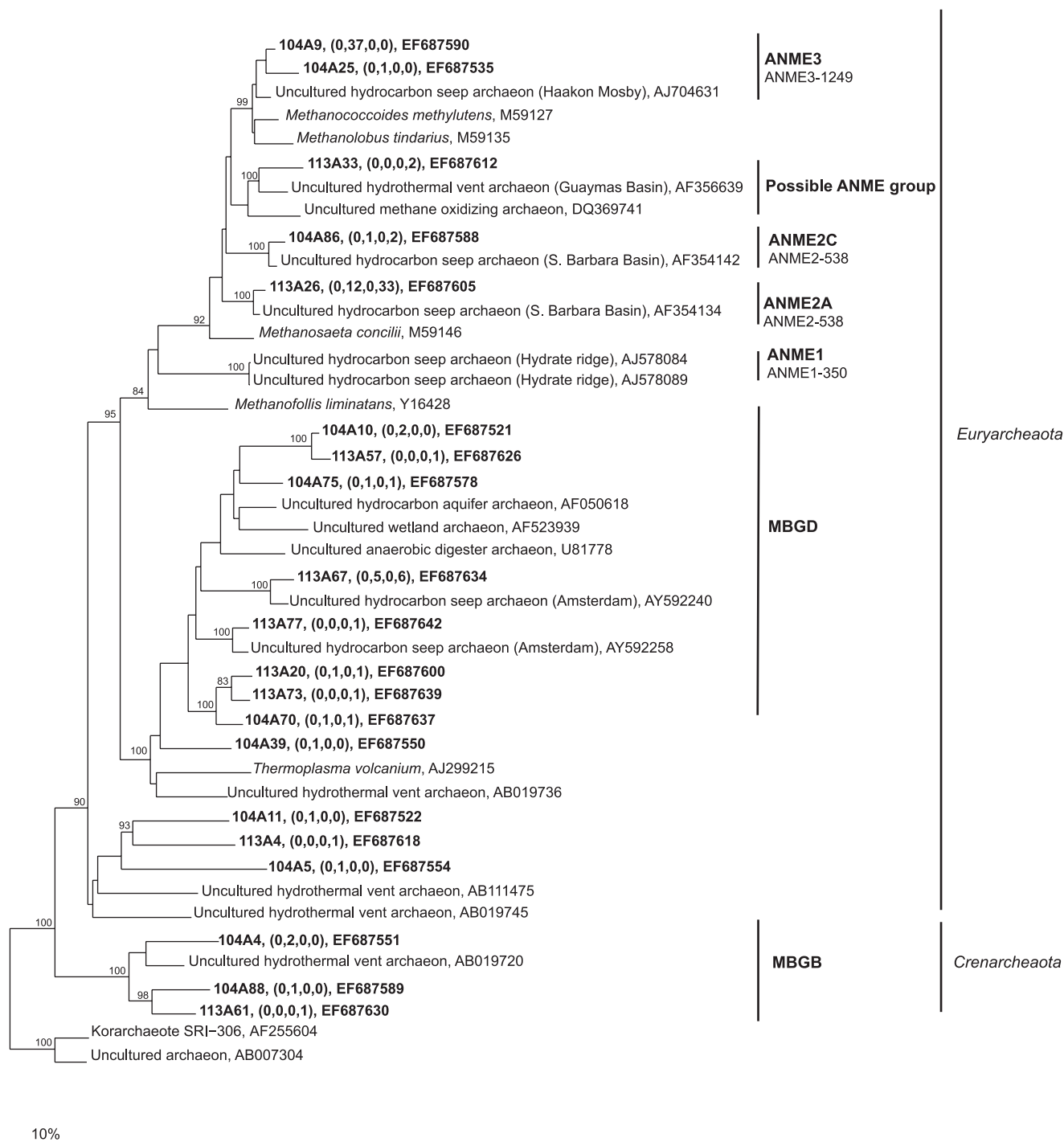


FIG. 9. Maximum parsimony tree of 16S rRNA gene sequences from *Archaea* obtained in this study, as well as from the GenBank database. The names in brackets are those of well-known cold seeps and hydrothermal vents. The bootstrap values at the nodes are percentages based on 500 replicates. Sequences from this study are indicated by bold type, and the numbers in parentheses indicate the numbers of sequences with 98% identity to the relevant sequences from the white mat, the sediment underlying the white mat, the orange mat, and the sediment underlying the orange mat. Only selected sequences are displayed. The sequence with accession number DQ369741 was excluded from the bootstrap analysis and added to the tree using the parsimony tool in ARB. Sequences that are targeted by ANME-1-350, ANME-2-538, and ANME-3-1249 are indicated.

to SR (1:1) (54). Hence, the sulfate-reducing community apparently utilized compounds other than methane or organic detritus (Table 3). High rates of SR that are severalfold greater than AOM rates are generally associated with seepage of

higher hydrocarbons and petroleum (28, 39, 58, 63; Omoregie et al., submitted). Besides methane, higher hydrocarbon compounds have been detected within the pore waters of Chefren and in the overlying water column and may fuel SR and Fe(III)

reduction (V. Mastalerz, unpublished data). Also, ANME-2 cells (Table 2) accounted for only 8 to 25% of the total cells in this zone, and ANME-3 cells accounted for only 6 to 27% of the total cells. These values, as well as the total cell numbers ($<10^9$ cells cm^{-3}), are lower than the values for other sites where AOM is the dominant biogeochemical process. Sites such as Hydrate Ridge, the Black Sea, and the Haakon Mosby mud volcano typically have ANME cell levels of $>10^9$ cells cm^{-3} , and these cells were found to comprise $>90\%$ of the total cells (7, 35).

Conclusion. This study elucidated some of the dominant microorganisms and processes involved in the formation of Fe(II)-oxidizing and sulfide-oxidizing mats at an active cold seep. Previously, these types of mats have been described only for hydrothermal vent settings, where sulfide and reduced iron were produced by seawater-rock interactions and advected by venting. Our findings suggest that such mats could also be fueled by microbial SR based on anaerobic hydrocarbon degradation maintained by relatively high fluid flow. Several questions still remain, such as the actual substrates fueling SR, the rates of microbial oxidation versus chemical Fe(II) and sulfide oxidation, the spatial relationship between the organisms that carry out these processes, and the ultimate fate of the end products [i.e., elemental S and Fe(III) (hydr)oxide].

ACKNOWLEDGMENTS

We thank the crews of the RV *L'Atalante* and the submersible *Nautile*, as well as the NAUTINIL scientific party, for their excellent work at sea. We thank Friederike Heinrich, Viola Beier, Tomas Wilkop, and Helge Niemann for their initial processing of the samples, Claus Burkhardt for help with the electron microscope, Stefan Sievert for informing us about "*Ca. Arcobacter sulfidicus*," Alban Ramette and Katrin Knittel for scientific suggestions, and Casey Hubert for helpful comments on the manuscript.

The work of A.K. was supported by an Emmy-Noether fellowship from the German Research Foundation (DFG). The work of E.O.O. and A.B. in the ESF EUROCORES MEDIFLUX was financially supported by ESF, DFG, and the Max Planck Society.

REFERENCES

- Aharon, P., and B. Fu. 2000. Microbial sulphate reduction rates and sulfur and oxygen isotope fractionations at oil and gas seeps in deepwater Gulf of Mexico. *Geochim. Cosmochim. Acta* **64**:233–246.
- Amann, R. I., L. Krumholz, and D. A. Stahl. 1990. Fluorescent-oligonucleotide probing of whole cells for determinative, phylogenetic, and environmental studies in microbiology. *J. Bacteriol.* **172**:762–770.
- Ashelford, K. E., N. A. Chuzhanova, J. C. Fry, A. J. Jones, and A. J. Weightman. 2005. At least 1 in 20 16S rRNA sequence records currently held in public repositories is estimated to contain substantial anomalies. *Appl. Environ. Microbiol.* **71**:7724–7736.
- Ashelford, K. E., N. A. Chuzhanova, J. C. Fry, A. J. Jones, and A. J. Weightman. 2006. New screening software shows that most recent large 16S rRNA gene clone libraries contain chimeras. *Appl. Environ. Microbiol.* **72**:5734–5741.
- Boetius, A., T. Ferdelman, and K. Lochte. 2000. Bacterial activity in sediments of the deep Arabian Sea in relation to vertical flux. *Deep-Sea Res.* **47**:2835–2875.
- Boetius, A., and K. Lochte. 1996. Effect of organic enrichments on hydrolytic potentials and growth of bacteria in deep-sea sediments. *Mar. Ecol. Prog. Ser.* **140**:239–250.
- Boetius, A., K. Ravensschlag, C. J. Schubert, D. Rickert, F. Widdel, A. Giesecke, R. Amann, B. B. Jørgensen, U. Witte, and O. Pfannkuche. 2000. A marine microbial consortium apparently mediating anaerobic oxidation of methane. *Nature* **407**:623–626.
- Boetius, A., S. Scheibe, A. Tselepidis, and H. Thiel. 1996. Microbial biomass and activities in deep-sea sediments of the Eastern Mediterranean: trenches are benthic hotspots. *Deep-Sea Res.* **43**:1439–1460.
- Burdige, D. J., and K. H. Nealson. 1986. Chemical and microbiological studies of sulfide-mediated manganese reduction. *Geomicrobiol. J.* **4**:361–387.
- Campbell, B. J., A. S. Engel, M. L. Porter, and K. Takai. 2006. The versatile epsilon-proteobacteria: key players in sulphidic habitats. *Nat. Rev. Microbiol.* **4**:458–468.
- Daims, H., A. Brühl, R. Amann, and K. H. Schleifer. 1999. The domain-specific probe EUB338 is insufficient for the detection of all Bacteria: development and evaluation of a more comprehensive probe set. *Syst. Appl. Microbiol.* **22**:434–444.
- De Lange, G. J., and H. J. Brumsack. 1998. The occurrence of gas hydrates in Eastern Mediterranean mud dome structures as indicated by porewater composition. *Geol. Soc. Spec.* **137**:167–175.
- Devereux, R., M. D. Kane, J. Winfrey, and D. A. Stahl. 1992. Genus- and group-specific hybridization probes for determinative and environmental studies of sulfate-reducing bacteria. *Syst. Appl. Microbiol.* **15**:601–609.
- Dupré, S., J. M. Woodside, J.-P. Foucher, G. de Lange, J. Mascle, A. Boetius, V. Mastalerz, A. Stadnitskaia, H. Ondreas, C. Huguen, F. Harmegnies, S. Gontharet, L. Loncke, E. Deville, H. Niemann, E. Omoregie, K. Olu-Le Roy, A. Fiala-Médioni, A. Dählmann, J.-C. Caprais, A. Prinzhofer, M. Sibuet, C. Pierre, J. Sinninghe Damsté, and N. S. Party. 2007. Seafloor geological studies above active gas chimneys off Egypt (Central Nile Deep Sea Fan). *Deep-Sea Res.* **54**:1146–1172.
- Eller, G., S. Stubner, and P. Frenzel. 2001. Group-specific 16S rRNA targeted probes for the detection of type I and type II methanotrophs by fluorescence in situ hybridisation. *FEMS Microbiol. Lett.* **198**:91–97.
- Emerson, D., and C. L. Moyer. 2002. Neutrophilic Fe-oxidizing bacteria are abundant at the Loihi Seamount hydrothermal vents and play a major role in Fe oxide deposition. *Appl. Environ. Microbiol.* **68**:3085–3093.
- Emerson, D., and N. P. Revsbech. 1994. Investigation of an iron-oxidizing microbial mat community located near Aarhus, Denmark: laboratory studies. *Appl. Environ. Microbiol.* **60**:4032–4038.
- Emerson, D., J. V. Weiss, and J. P. Megonigal. 1999. Iron-oxidizing bacteria are associated with ferric hydroxide precipitates (Fe-plaque) on the roots of wetland plants. *Appl. Environ. Microbiol.* **65**:2758–2761.
- Finster, K., W. Liesack, and B. Thamdrup. 1998. Elemental sulfur and thiosulfate disproportionation by *Desulfocapsa sulfoexigens* sp. nov., a new anaerobic bacterium isolated from marine surface sediment. *Appl. Environ. Microbiol.* **64**:119–125.
- Grasshoff, K., M. Ehrhardt, and K. Kremling. 1983. Methods of seawater analysis, p. 419. Verlag Chemie, Weinheim, Germany.
- Hinrichs, K.-U., and A. Boetius. 2002. The anaerobic oxidation of methane: new insights in microbial ecology and biogeochemistry, p. 457–477. *In* G. Wefer, D. Billett, D. Hebbeln, B. B. Jørgensen, M. Schlüter, and T. Van Weering (ed.), *Ocean margin systems*. Springer-Verlag, Berlin, Germany.
- Inagaki, F., M. M. M. Kuypers, U. Tsunogai, J. Ishibashi, K. Nakamura, T. Treude, S. Ohkubo, M. Nakaseama, K. Gena, H. Chiba, H. Hirayama, T. Nunoura, K. Takai, B. B. Jørgensen, K. Horikoshi, and A. Boetius. 2006. Microbial community in a sediment-hosted CO₂ lake of the southern Okinawa Trough hydrothermal system. *Proc. Natl. Acad. Sci. USA* **103**:14164–14169.
- Ishii, K., M. Mussmann, B. J. MacGregor, and R. Amann. 2004. An improved fluorescence in situ hybridization protocol for the identification of bacteria and archaea in marine sediments. *FEMS Microbiol. Ecol.* **50**:203–213.
- Iversen, N., and T. H. Blackburn. 1981. Seasonal rates of methane oxidation in anoxic marine sediments. *Appl. Environ. Microbiol.* **41**:1295–1300.
- Iversen, N., and B. B. Jørgensen. 1993. Diffusion coefficients of sulfate and methane in marine sediments influence of porosity. *Geochim. Cosmochim. Acta* **57**:571–578.
- James, R. E., and F. G. Ferris. 2004. Evidence for microbial-mediated iron oxidation at a neutrophilic groundwater spring. *Chem. Geol.* **212**:301.
- Jørgensen, B. B. 1978. A comparison of methods for the quantification of bacterial sulfate reduction in coastal marine sediments. Measurement with radiotracer techniques. *Geomicrobiol. J.* **1**:11–27.
- Joye, S. B., A. Boetius, B. N. Orcutt, J. P. Montoya, H. N. Schulz, M. J. Erickson, and S. K. Loge. 2004. The anaerobic oxidation of methane and sulfate reduction in sediments from Gulf of Mexico cold seeps. *Chem. Geol.* **205**:219–238.
- Kalanetra, K. M., S. B. Joye, N. R. Sunseri, and D. C. Nelson. 2005. Novel vacuolate sulfur bacteria from the Gulf of Mexico reproduce by reductive division in three dimensions. *Environ. Microbiol.* **7**:1451–1460.
- Kallmeyer, J., T. G. Ferdelman, A. Weber, H. Fossing, and B. B. Jørgensen. 2004. Evaluation of a cold chromium distillation procedure for recovering very small amounts of radiolabeled sulfide related to sulfate reduction measurements. *Limnol. Oceanogr. Methods* **2**:171–180.
- Kane, M. D., L. K. Poulsen, and D. A. Stahl. 1993. Monitoring the enrichment and isolation of sulfate-reducing bacteria by using oligonucleotide hybridization probes designed from environmentally derived 16S rRNA sequences. *Appl. Environ. Microbiol.* **59**:682–686.
- Kasten, S., and B. B. Jørgensen. 2000. Sulfate reduction in marine sediments, p. 263–281. *In* H. D. Schulze and M. Zabel (ed.), *Marine geochemistry*. Springer, Berlin, Germany.
- Kennedy, C. B., S. D. Scott, and F. G. Ferris. 2003. Characterization of

- bacteriogenic iron oxide deposits from Axial Volcano, Juan de Fuca Ridge, northeast Pacific Ocean. *Geomicrobiol. J.* **20**:199–214.
34. Kennedy, C. B., S. D. Scott, and F. G. Ferris. 2003. Ultrastructure and potential sub-seafloor evidence of bacteriogenic iron oxides from axial volcano, Juan de Fuca Ridge, North-east Pacific Ocean. *FEMS Microbiol. Ecol.* **43**:247–254.
 35. Knittel, K., A. Boetius, A. Lemke, H. Eilers, K. Lochte, O. Pfannkuche, P. Linke, and R. Amann. 2003. Activity, distribution, and diversity of sulfate reducers and other bacteria in sediments above gas hydrate (Cascadia margin, Oregon). *Geomicrobiol. J.* **20**:269–294.
 36. Knittel, K., T. Losekann, A. Boetius, R. Kort, and R. Amann. 2005. Diversity and distribution of methanotrophic archaea at cold seeps. *Appl. Environ. Microbiol.* **71**:467–479.
 37. Krom, M. D., S. Brenner, L. Israilov, and B. Krumgalz. 1991. Dissolved nutrients, preformed nutrients and calculated elemental ratios in the south-east Mediterranean Sea. *Oceanol. Acta* **14**:189–194.
 38. Lane, D., B. Pace, G. Olsen, D. Stahl, M. Sogin, and N. Pace. 1985. Rapid determination of 16S ribosomal RNA sequences for phylogenetic analyses. *Proc. Natl. Acad. Sci. USA* **82**:6955–6959.
 39. Lloyd, K. G., L. Lapham, and A. Teske. 2006. Anaerobic methane-oxidizing community of ANME-1b archaea in hypersaline Gulf of Mexico sediments. *Appl. Environ. Microbiol.* **72**:7218–7230.
 40. Loncke, L., V. Gaullier, J. Mascle, B. Vendeville, and L. Camera. 2006. The Nile deep-sea fan: an example of interacting sedimentation, salt tectonics, and inherited subsalt paleotopographic features. *Mar. Pet. Geol.* **23**:297–315.
 41. Lösekann, T., K. Knittel, T. Nadalig, B. Fuchs, H. Niemann, A. Boetius, and R. Amann. 2007. Diversity and abundance of aerobic and anaerobic methane oxidizers at the Haakon Mosby Mud Volcano, Barents Sea. *Appl. Environ. Microbiol.* **73**:3348–3362.
 42. Lovley, D. R., E. J. P. Phillips, D. J. Lonergan, and P. K. Widman. 1995. Fe(III) and S⁰ reduction by *Pelobacter carbinolicus*. *Appl. Environ. Microbiol.* **61**:2132–2138.
 43. Lovley, D. R., E. E. Roden, E. J. P. Phillips, and J. C. Woodward. 1993. Enzymatic iron and uranium reduction by sulfate-reducing bacteria. *Mar. Geol.* **113**:41.
 44. Ludwig, W., O. Strunk, R. Westram, L. Richter, H. Meier, Yadhukumar, A. Buchner, T. Lai, S. Steppi, G. Jobb, W. Forster, I. Brettske, S. Gerber, A. W. Ginhart, O. Gross, S. Grumann, S. Hermann, R. Jost, A. König, T. Liss, R. Lussmann, M. May, B. Nonhoff, B. Reichel, R. Strehlow, A. Stamatakis, N. Stuckmann, A. Vilbig, M. Lenke, T. Ludwig, A. Bode, and K.-H. Schleifer. 2004. ARB: a software environment for sequence data. *Nucleic Acids Res.* **32**:1363–1371.
 45. Luff, R., and K. Wallmann. 2003. Fluid flow, methane fluxes, carbonate precipitation and biogeochemical turnover in gas hydrate-bearing sediments at Hydrate Ridge, Cascadia Margin: numerical modeling and mass balances. *Geochim. Cosmochim. Acta* **67**:3403–3421.
 46. Manz, W., R. Amann, W. Ludwig, M. Wagner, and K. H. Schleifer. 1992. Phylogenetic oligodeoxynucleotide probes for the major subclasses of proteobacteria: problems and solutions. *Syst. Appl. Microbiol.* **15**:593–600.
 47. Mascle, J., L. Loncke, and L. Camera. 2005. Geophysical evidences of fluid seepages and mud volcanoes on the Egyptian continental margin (Eastern Mediterranean). *Boll. Soc. Geol. Ital.* **2005**(4):127–134.
 48. Mascle, J., O. Sardou, L. Loncke, S. Migeon, L. Camera, and V. Gaullier. 2006. Morphostructure of the Egyptian continental margin: insights from swath bathymetry surveys. *Mar. Geophys. Res.* **27**:49–59.
 49. Massana, R., A. E. Murray, C. M. Preston, and E. F. DeLong. 1997. Vertical distribution and phylogenetic characterization of marine planktonic Archaea in the Santa Barbara Channel. *Appl. Environ. Microbiol.* **63**:50–56.
 50. Mau, S., H. Sahling, G. Rehder, E. Suess, P. Linke, and E. Soeding. 2006. Estimates of methane output from mud extrusions at the erosive convergent margin off Costa Rica. *Mar. Geol.* **225**:129–144.
 51. Michaelis, W., R. Seifert, K. Nauhaus, T. Treude, V. Thiel, M. Blumenberg, K. Knittel, A. Gieseke, K. Peterknecht, T. Pape, A. Boetius, A. Aman, B. B. Jørgensen, F. Widdel, J. Peckmann, N. V. Pimenov, and M. Gulin. 2002. Microbial reefs in the Black Sea fueled by anaerobic oxidation of methane. *Science* **297**:1013–1015.
 52. Mills, H. J., R. J. Martinez, S. Story, and P. A. Sobczyk. 2005. Characterization of microbial community structure in Gulf of Mexico gas hydrates: comparative analysis of DNA- and RNA-derived clone libraries. *Appl. Environ. Microbiol.* **71**:3235–3247.
 53. Muyzer, G., A. Teske, C. O. Wirsen, and H. W. Jannasch. 1995. Phylogenetic relationships of Thiomicrospira species and their identification in deep-sea hydrothermal vent samples by denaturing gradient gel-electrophoresis of 16S rDNA fragments. *Arch. Microbiol.* **164**:165–172.
 54. Nauhaus, K., A. Boetius, M. Krüger, and F. Widdel. 2002. In vitro demonstration of anaerobic oxidation of methane coupled to sulphate reduction in sediment from marine gas hydrate area. *Environ. Microbiol.* **4**:298–305.
 55. Neef, A. 1997. Anwendung der in situ-Einzell-Identifizierung von Bakterien zur Populations-Analyse in komplexen mikrobiellen Biozönosen. Technische Universität München, München, Germany.
 56. Nelson, D. C., C. O. Wirsen, and H. W. Jannasch. 1989. Characterization of large, autotrophic *Beggiatoa* spp. abundant at hydrothermal vents of the Guaymas Basin. *Appl. Environ. Microbiol.* **55**:2909–2917.
 57. Neubauer, S. C., D. Emerson, and J. P. Megonigal. 2002. Life at the energetic edge: kinetics of circumneutral iron oxidation by lithotrophic iron-oxidizing bacteria isolated from the wetland-plant rhizosphere. *Appl. Environ. Microbiol.* **68**:3988–3995.
 58. Niemann, H., J. Duarte, C. Hensen, E. Omereg, V. H. Magalhaes, M. Elvert, L. M. Pinheiro, A. Kopf, and A. Boetius. 2006. Microbial methane turnover at mud volcanoes of the Gulf of Cadiz. *Geochim. Cosmochim. Acta* **70**:5336.
 59. Niemann, H., T. Losekann, D. de Beer, M. Elvert, T. Nadalig, K. Knittel, R. Amann, E. J. Sauter, M. Schluter, M. Klages, J. P. Foucher, and A. Boetius. 2006. Novel microbial communities of the Haakon Mosby mud volcano and their role as a methane sink. *Nature* **443**:854.
 60. Nijenhuis, I. A., H. J. Bosch, J. S. Sinninghe Damsté, H. J. Brumsack, and G. J. De Lange. 1999. Organic matter and trace element rich sapropels and black shales: a geochemical comparison. *Earth Planet. Sci. Lett.* **169**:277–290.
 61. Nikolaus, R., J. W. Ammerman, and I. R. MacDonald. 2003. Distinct pigmentation and trophic modes in *Beggiatoa* from hydrocarbon seeps in the Gulf of Mexico. *Aquat. Microb. Ecol.* **32**:85–93.
 62. Olu-Le Roy, K., M. Sibuet, A. Fiala-Medioni, S. Gofas, C. Salas, A. Mariotti, J. P. Foucher, and J. Woodside. 2004. Cold seep communities in the deep eastern Mediterranean Sea: composition, symbiosis and spatial distribution on mud volcanoes. *Deep-Sea Res.* **51**:1915–1936.
 63. Orcutt, B., A. Boetius, M. Elvert, V. Samarkin, and S. B. Joye. 2005. Molecular biogeochemistry of sulfate reduction, methanogenesis and the anaerobic oxidation of methane at Gulf of Mexico cold seeps. *Geochim. Cosmochim. Acta* **69**:4267–4281.
 64. Reitz, A., J. Thomson, G. J. de Lange, and C. Hensen. 2006. Source and development of large manganese enrichments above eastern Mediterranean sapropel S1. *Paleoceanography* **21**:PA3007.
 65. Robinson, C. A., J. M. Bernhard, L. A. Levin, G. F. Mendoza, and J. K. Blanks. 2004. Surficial hydrocarbon seep infauna from the Blake Ridge (Atlantic Ocean, 2150 m) and the Gulf of Mexico (690–2240 m). *Mar. Ecol. Prog. Ser.* **25**:313–336.
 66. Roden, E. E., and D. R. Lovley. 1993. Dissimilatory Fe(III) reduction by the marine microorganism *Desulfuromonas acetoxidans*. *Appl. Environ. Microbiol.* **59**:734–742.
 67. Sahling, H., D. Rickert, R. W. Lee, P. Linke, and E. Suess. 2002. Macrofaunal community structure and sulfide flux at gas hydrate deposits from the Cascadia convergent margin, NE Pacific. *Mar. Ecol. Prog. Ser.* **231**:121–138.
 68. Sassen, R., S. L. Losh, I. L. Cathles, H. H. Roberts, J. K. Whelan, A. V. Milkov, S. T. Sweet, and D. A. DeFreitas. 2001. Massive vein-filling gas hydrate: relation to ongoing gas migration from the deep subsurface in the Gulf of Mexico. *Mar. Pet. Geol.* **18**:551.
 69. Sassen, R., H. H. Roberts, P. Aharon, J. Larkin, E. W. Chinn, and R. Carney. 1993. Chemosynthetic bacterial mats at cold hydrocarbon seeps, Gulf of Mexico continental slope. *Org. Geochem.* **20**:77.
 70. Schloss, P. D., B. R. Larget, and J. Handelsman. 2004. Integration of microbial ecology and statistics: a test to compare gene libraries. *Appl. Environ. Microbiol.* **70**:5485–5492.
 71. Sibuet, M., and K. Olu. 1998. Biogeography, biodiversity and fluid dependence of deep-sea cold-seep communities at active and passive margins. *Deep-Sea Res.* **45**:517–567.
 72. Sievert, S. M., E. B. A. Wieringa, C. O. Wirsen, and C. D. Taylor. 2006. Growth and mechanism of filamentous-sulfur formation by *Candidatus Arcobacter sulfidicus* in opposing oxygen-sulfide gradients. *Environ. Microbiol.* **9**:271–276.
 73. Snaidr, J., R. Amann, I. Huber, W. Ludwig, and K. H. Schleifer. 1997. Phylogenetic analysis and in situ identification of bacteria in activated sludge. *Appl. Environ. Microbiol.* **63**:2884–2896.
 74. Staudigel, H., S. R. Hart, A. Pile, B. E. Bailey, E. T. Baker, S. Brooke, D. P. Connelly, L. Hauke, C. R. German, I. Hudson, D. Jones, A. A. P. Koppers, J. Konter, R. Lee, T. W. Pietsch, B. M. Tebo, A. S. Templeton, R. Zierenberg, and C. M. Young. 2006. Vailulu'u Seamount, Samoa: life and death on an active submarine volcano. *Proc. Natl. Acad. Sci. USA* **103**:6448–6453.
 75. Stoeker, K., B. Bendinger, B. Schöning, P. H. Nielsen, J. L. Nielsen, C. Baranyi, E. R. Toenshoff, H. Daims, and M. Wagner. 2006. Cohn's *Crenothrix* is a filamentous methane oxidizer with an unusual methane monooxygenase. *Proc. Natl. Acad. Sci. USA* **103**:2363–2367.
 76. Straub, K. L., and B. Schink. 2004. Ferrihydrite-dependent growth of *Sulfospirillum deleyianum* through electron transfer via sulfur cycling. *Appl. Environ. Microbiol.* **70**:5744–5749.
 77. Taylor, C. D., and C. O. Wirsen. 1997. Microbiology and ecology of filamentous sulfur formation. *Science* **277**:1483–1485.
 78. Taylor, C. D., C. O. Wirsen, and F. Gaill. 1999. Rapid microbial production of filamentous sulfur mats at hydrothermal vents. *Appl. Environ. Microbiol.* **65**:2253–2255.
 79. Taylor, S. W., C. R. Lange, and E. A. Lesold. 1997. Biofouling of contaminated ground-water recovery wells: characterization of microorganisms. *Ground Water* **35**:973–980.

80. **Thamdrup, B., H. Fossing, and B. B. Jørgensen.** 1994. Manganese, iron, and sulfur cycling in a coastal marine sediment, Aarhus Bay, Denmark. *Geochim. Cosmochim. Acta* **58**:5115–5129.
81. **Treude, T., A. Boetius, K. Knittel, K. Wallmann, and B. B. Jørgensen.** 2003. Anaerobic oxidation of methane above gas hydrates at Hydrate Ridge, NE Pacific Ocean. *Mar. Ecol. Prog. Ser.* **264**:1–14.
82. **Treude, T., K. Knittel, M. Blumenberg, R. Seifert, and A. Boetius.** 2005. Subsurface microbial methanotrophic mats in the Black Sea. *Appl. Environ. Microbiol.* **71**:6375–6378.
83. **Treude, T., J. Niggemann, J. Kallmeyer, P. Wintersteller, C. J. Schubert, A. Boetius, and B. B. Jørgensen.** 2005. Anaerobic oxidation of methane and sulfate reduction along the Chilean continental margin. *Geochim. Cosmochim. Acta* **69**:2767–2779.
84. **van Santvoort, P. J. M., and G. J. deLange.** 1996. Messinian salt fluxes into the present-day eastern Mediterranean: implications for budget calculations and stagnation. *Mar. Geol.* **132**:241–251.
85. **van Santvoort, P. J. M., G. J. deLange, J. Thomson, H. Cussen, T. R. S. Wilson, M. D. Krom, and K. Strohle.** 1996. Active post-depositional oxidation of the most recent sapropel (S1) in sediments of the eastern Mediterranean Sea. *Geochim. Cosmochim. Acta* **60**:4007–4024.
86. **van Veen, W. L., E. G. Mulder, and M. Deinema.** 1978. The *Sphaerotilus-Leptothrix* group of bacteria. *Microbiol. Rev.* **42**:329–356.
87. **Vigliotta, G., E. Nutricati, E. Carata, S. M. Tredici, M. De Stefano, P. Pontieri, D. R. Massardo, M. V. Prati, L. De Bellis, and P. Alifano.** 2007. *Clonothrix fusca* Roze 1896, a filamentous, sheathed, methanotrophic γ -proteobacterium. *Appl. Environ. Microbiol.* **73**:3556–3565.
88. **Volker, H., R. Schweisfurth, and P. Hirsch.** 1977. Morphology and ultrastructure of *Crenothrix polyspora* Cohn. *J. Bacteriol.* **131**:306–313.
89. **Wallner, G., I. Steinmetz, D. Bitter-Suermann, and R. Amann.** 1996. Flow cytometric analysis of activated sludge with rRNA-targeted probes. *Appl. Environ. Microbiol.* **19**:569–576.
90. **Woodside, J. M.** 2000. Linking Mediterranean brine pools and mud volcanism. *EOS Trans. Am. Geophys. Union* **81**:625, 631–633.
91. **Woodside, J. M., and A. V. Volgin.** 1996. Brine pools associated with Mediterranean Ridge mud diapirs: an interpretation of echo-free patches in deep tow sidescan sonar data. *Mar. Geol.* **132**:55–61.
92. **Zitter, T. A. C., C. Huguen, and J. M. Woodside.** 2005. Geology of mud volcanoes in the eastern Mediterranean from combined sidescan sonar and submersible surveys. *Deep-Sea Res.* **52**:457–475.